Irrigation Science (2025) 43:613–636
https://doi.org/10.1007/s00271-025-01012-1

ORIGINAL PAPER

Altered calcium and potassium distribution maps in tomato tissues cultivated under salinity: studies using X-ray fluorescence (XFM) microscopy

Abdullah Al Hosni[1,5] · Daryl C. Joyce[1,3] · Mal Hunter[2] · Melinda Perkins[3] · Rashid Al Yahyai[4]

Received: 30 October 2024 / Accepted: 17 March 2025 / Published online: 19 April 2025
© The Author(s) 2025

Abstract

Calcium (Ca^{2+}) distribution into relatively low-transpiring fruit versus relatively high-transpiring leaves is of concern to the fruit industry. Ca^{2+} uptake is further compromised under salinity through antagonistic competition with sodium (Na^{+}). Herein, X-Ray Fluorescence (XFM) was applied to elucidate *in-situ* localization and distribution patterns of Ca^{2+} and potassium (K^{+}) in tomato leaflet and fruit tissues under salinity versus non-saline controls. Leaflet Ca^{2+} signal was up to 7 times higher than that in fruit. Highest Ca^{2+} hotspots were in leaflet blades, notably at their margins. XFM spatial maps revealed striking contrasts in K^{+} versus Ca^{2+} patterns along proximal–distal mesocarp tissues. Under compressive stress, proximal fruit flesh tissues were firmer, stiffer and showed higher resilience to mechanical deformation than distal tissues. This intrinsic mechanical gradient property was positively correlated with Ca^{2+} locality. Added Ca^{2+} ameliorated mechanical failure induced by Na^{+} and restored fruit firmness, but not stiffness and peak force. The exocarp had the strongest Ca^{2+} signal in fruit tissue. The weakest was in the locular cavity. Ca^{2+} in Blossom End Rot (BER) affected tissue was up to fourfold that in immediately surrounding sound tissue, reflecting cell wall collapse. New insights reported here into Ca^{2+} and K^{+} dynamics in tomato mesocarp under salinity offer improved understanding of fruit mechanical properties and Ca^{2+}-deficiency.

Introduction

Calcium (Ca^{2+}) is an essential element for plant growth and productivity. It is involved in signal transduction and uptake of nutrients across cell membranes (Park et al. 2005; Bose et al. 2011; Hocking et al. 2016). Ca^{2+} also mediates cell membrane integrity and cross links pectin in cell walls such as to enhance load-bearing properties of fruit (Peaucelle et al. 2012; Hyodo et al. 2013; Braidwood et al. 2014). Normal fruit development requires constant supply of Ca^{2+}. As a phloem-immobile element, Ca^{2+} taken up by roots moves via the xylem into aboveground structures, including fruit, by bulk water flow driven by transpiration (Montanaro et al. 2010; Indeche et al. 2020). In plant tissues, Ca^{2+} may bind to cell walls and membranes, remain free in the apoplast or be stored in the cytosol or cellular organelles such as the vacuole (de Freitas et al. 2012; Stael et al. 2012). The cell wall apoplast is a main Ca^{2+} storage site in plant cells (Costa et al. 2018). To a significant degree, bound Ca^{2+} determines fruit mechanical properties (Cybulska et al. 2011).

The extracellular matrix comprising the cell wall is mainly comprised cellulose, hemicellulose, and lignin with a pectin network matrix (Tenhaken 2015). Ca^{2+} binds to negatively charged carboxyl groups in the polygalacturonic acid backbone of pectin within the middle lamella and cell wall. Cybulska et al. (2011) noted that Ca^{2+}-pectin maintains fruit cell functioning, structure, and stability via underpinning cell wall integrity. Ca^{2+} is held in cell walls according to the "egg-box" model wherein pectin molecules are cross-linked by Ca^{2+} bridges. The tight bonding confers tissue strength (Peaucelle et al. 2012). The Ca^{2+} bridges between

✉ Abdullah Al Hosni
a.alhosni@uq.net.au

1 School of Agriculture and Food Sustainability, The University of Queensland, Gatton, QLD 4343, Australia

2 School of Agriculture and Food Sustainability, The University of Queensland, Brisbane, QLD 4067, Australia

3 Gatton Research Facility, Queensland Department of Agriculture and Fisheries, Gatton, QLD 4343, Australia

4 College of Agricultural and Marine Sciences, Sultan Qaboos University, Muscat, OM 123, Oman

5 Oman Botanic Garden, Ministry of Heritage and Tourism, Muscat, OM 122, Oman

free carboxyl groups of pectin chains act to gel fruit tissues (Wang et al. 2018). Depletion of Ca^{2+} in the apoplast contributes to softening of the cell structures because it limits Ca^{2+} cross-linking with the carboxyl groups of pectin chains that otherwise form 'egg box' structures (Peaucelle et al. 2015; Wang et al. 2018).

Tomato and pepper blossom end-rot (BER), apple bitter pit, pear fruit hard-end celery blackheart, mango soft nose, jelly seed, and stem end cavity and lettuce tipburn disorders in fresh produce have been linked to Ca^{2+}-deficiency (Taylor and Locascio 2004; Ho and White 2005). Fruits that develop Ca^{2+}-deficiency disorders tend to have lower Ca^{2+} concentrations and plants grown under deficit Ca^{2+} nutrition have higher incidence of such disorders. Despite long-standing awareness, the issue remains a practical problem and inflicts substantial losses in the fresh produce industry. BER in tomato, for instance, can afflict economic losses up to 50% of the total production under severe abiotic stress conditions (Taylor and Locascio 2004).

Despite many studies on fruit biomechanics (Li and Thomas 2014; Winisdorffer et al. 2015; Besada et al. 2016; Liu et al. 2019; An et al. 2020), in-depth study as to possible influences of Na^{+} on plant tissue mechanical properties is wanting, especially as ~40% of irrigated agriculture is expected to be affected by salinity by 2050 (Hrmova and Gilliham 2018). Na^{+} alters nutrient uptake patterns (Vang-Petersen 1980; Moles et al. 2019), damages cells (Flowers et al. 2015), disrupts plasma membrane permeability (Tuna et al. 2007), causes cellular toxicity (Munns and Tester 2008; Flowers et al. 2015) and reduces plant Ca^{2+} levels (Islam et al. 2018; Moles et al. 2019; Costan et al. 2020). Ca^{2+} is a pectin gelling or linking agent and so mediates plant tissue mechanical properties (Cybulska et al. 2011). As noted above, Ca^{2+} ions crosslink the negatively charged carboxylic groups in pectin that mediate load-bearing properties and cell wall biomechanics (Bose et al. 2011; Tenhaken 2015). When Na^{+} displaces pectin-bound Ca^{2+} it disrupts the pectin cross linking (Feng et al. 2018). Na^{+} directly impacted the mechanical properties of *Arabidopsis thaliana* root cell walls caused by N^{+} apoplastic toxicity and cellular bursting due to disruption of cellulose being the wall load-bearing material. This study highlighted the negative effect of the Na^{+} on cell wall stiffness. Such observations raise more questions as to the impacts of Na^{+} on fruit Ca^{2+} import, including how fruit with high Na^{+} concentrations react to compression and impact forces.

Mechanical behaviour of fruit tissue has been the subject of many investigations (García et al. 1995; Alamar et al. 2008; Li et al. 2012; Zipori et al. 2014; Stopa et al. 2018; Giongo et al. 2019; Liu et al. 2019). However, relatively little is known as to how in vivo fruit mechanical properties (e.g., tomato firmness, stiffness, puncture resistance) alter with varying Na^{+} and Ca^{2+} supply. Fruits are inherently dynamic and highly complex biologically, being comprised of varied tissue types. The main three layers of the pericarp are exocarp, mesocarp, and endocarp (Cerri and Reale 2020), which have differing structural features and mechanical properties. Each tissue type has distinct functions and roles and may promote, sustain, restrict, or counteract mechanical forces differently (Diels et al. 2019). Thick walled exocarp cells offer flexible or extensible mechanical support and maintain fruit integrity. Thereby, the exocarp provides protection against puncture, but not to the same extent against impact forces that transmit to underlying thin and inelastic parenchyma cells (Li et al. 2012). Although the mesocarp determines overall mechanical properties of fruit because it typically represents the bulk of the edible part of fruits f horticulture, there are few studies of mesocarp mechanics as influenced by Na^{+} and Ca^{2+} (Petersen et al. 1998; Ruiz et al. 2015; Tang et al. 2020). Mapping fruit mechanical properties like firmness, stiffness, and puncture resistance across fruit mesocarp tissues grown under different Ca^{2+} and Na^{+} regimes and relating them to Ca^{2+} spatial location at high detection sensitivity down to sub-parts-per-million is thus potentially informative. Further, physiological mechanisms of Ca^{2+} distribution in the mesocarp at the tissue level have not been comprehensively investigated. Sophisticated methodologies can be called up to investigate potential Ca^{2+} hotspots, where Ca^{2+} mostly trapped, and localized Ca^{2+}-deficiency.

Conventional approaches to assessing biological samples for nutrients typically cannot reveal relationships between the presence of nutrients in the rooting medium and within reproductive organs either statically as fruit grow or dynamically at tissue level. Inductively coupled plasma mass spectrometry (ICP-MS) is used widely to measure concentrations of nutrient elements, including Ca^{2+}, in biological tissues. However, on a fine scale ICP-MS does not address spatial nutrient distribution within tissues. High resolution is, however, desired to understand Ca^{2+} distribution between and within tissues. That is, high spatial resolution maps are needed for deeper insight into movement of mineral elements and to discern how nutrients interact at specific locations. Synchrotron XFM has emerged as a tool to provide multi-elemental qualitative and quantitative analysis towards understanding movement and partitioning of nutrients (van der Ent et al. 2018).

This present study generated XFM maps to characterise the distribution of Ca^{2+} and K^{+} under Na^{+} (saline) conditions with Ca^{2+} supply to tomato leaves and fruit. The working hypothesis was that Ca^{2+} supplementation in irrigation solution would displace Na^{+} in cell walls to enhance flesh mechanical properties. For the second experiment, it was hypothesized that enhanced Ca^{2+} supplementations would ameliorate Na^{+} toxicity fruit tissues via increased Ca^{2+} translocation and partitioning and decreased Na^{+} uptake

and improved K^+ homeostasis. To investigate these hypotheses a combination of Inductively Coupled Plasma Mass Spectrometry (ICP-MS) and micro-XFM was employed to reveal nutrient spatial distributions within and among tomato fruit tissues.

Materials and methods

Experiment one: nutrients and mechanical properties

Experimental area and planting material

Two experiments were conducted in 2018 and 2019, respectively. Tomato plants (*Solanum lycopersicum*) were grown under glasshouse conditions at The University of Queensland, Gatton (−27.55402 latitude, 152.33686 longitude). Daily average vapour pressure deficit (VPD) was 1.57 kPa, temperature was 23.5°C, and relative humidity was 57.3%. Tomato cv. Roma VF, an important processing variety, was chosen for studying morphological characteristics and Ca^{2+} distribution patterns (Riboldi et al. 2018) in response to saline conditions. This determinate variety completes its life cycle in a relatively short time. cv. Roma fruit have three locules. In a study on four locule tomato fruit, significant mechanical damage was reported in terms of plastic strain energy, *E*p, peak force, *F*max and degree of elasticity upon robotic handling. Three locule varieties are considered more robust (Li et al. 2010).

The tomato seedlings were raised in trays of 1:1 (v/v) peat-perlite. The substrate media was kept consistently moist by periodic sprinkler irrigation. To help avoid dehydration, seeds were covered with dry vermiculite. Two weeks after sowing, the seedlings were transplanted into individual 4L plastic ANOVApot® pots (Hunter and Scattini 2014; Hunter et al. 2018) containing sand. The coarse sand (pH 7.4; EC 0.1 dS/m) was initially steam sterilized at 65 °C for 2 h. Basal fertilizer per pot was 'Osmocote Exact' (16 g 3–4 month slow-release; (Atkinson et al. 2011). According to label, the elemental composition (%) of 'Osmocote Exact' is N 16, P 9, K^+ 12, Mg^{2+} 2; Fe 0.45; Mn^{2+} 0.06, B 0.02; Cu 0.05; Mo 0.02, and Zn^{2+} 0.015. The concentration of Ca^{2+} and Na^+ are expressed in mM in experimental design and treatments section.

Each planted ANOVApot® was placed inside another ANOVApot® thereby forming a Twinpot Water Management System (Hunter and Scattini 2014). In this system a constant water table is maintained in the lower pot by an internal float valve connected to an external 4 L translucent plastic reservoir within and for which the water level can be monitored. Normal drainage through a central basal hole in the lower pot is prevented by plugging with silicone. Drainage that might be needed in the case of valve failure can occur through a 6 mm diameter hole at a height in the lower pot level with the top of the valve. The water in the lower pot transfers into the bottom of the upper pot via capillary tape draped over the centrally placed valve capped with an 80 mm square of sheet of plastic Corflute™. During plant transpiration increasing water tension is created in the sand medium of the upper pot and water moves up from the constant water table in the lower pot through the capillary tape and into the capillary tape covered sand filled hole in the base of the upper pot. Non-transpirational water loss was minimized by covering the upper pot surface with silver coated plastic film, SILVERWRAP™ BREATHER'.

Experimental design and treatments

The main experiment was conducted in the wake of two preliminary experiments to establish appropriate Ca^{2+} and Na^+ concentrations in irrigation water that does not incur toxicity that led to poor fruit production. After establishing the upper concentration allowing growth, nine different Ca^{2+} and Na^+ level treatments were chosen: 6 mM Ca^{2+} and no Na^+, control; 6 mM Ca^{2+} and 16 mM Na^+; 6 mM Ca^{2+} and 32 mM Na^+;12 mM Ca^{2+} and no Na^+; 12 mM Ca^{2+} and 16 mM Na^+; 12 mM Ca^{2+} and 32 mM Na^+; 18 mM Ca^{2+} and no Na^+; 18 mM Ca^{2+} and 16 mM Na^+; and, 18 mM Ca^{2+} and 32 mM Na^+.

Controls were determined after De Kreij et al. (1997) with the standard concentration of Ca^{2+} in the nutrient solution for tomato cultivation from $CaSO_4{\cdot}2H_2O$ being between 5.4 and 6 mM. The measured concentration within the root zone was between 6 and 10 mM. Replication was five-fold for a total of 45 plants. $CaSO_4.2H_2O$ was the Ca^{2+} supply in the irrigation solution and NaCl for Na^+ and experiment design was completely randomized. To avoid osmotic shock, plants were supplied with 6 mM Ca^{2+} in the first 2 weeks. NaCl was then introduced and incrementally increased 50% of the target solution concentration after 3 days and 100% by the 7th day. Thereafter, the target NaCl level was maintained for the remainer of the experiment by refilling the reservoir with Ca^{2+} and Na^+ deionized water solutions. The experiment was conducted over 90 days, 76 of which involved constant supply of Ca^{2+} or Na^+ or the two ions in combination.

Water uptake and vegetative growth

Cumulative plant transpiration rate was estimated by calculating and progressively summing daily transpired water for each plant. Water used was determined at 9 am daily by recording and calculating the drop in water level in the reservoir in mL over the previous 24 h. Biomass accumulation over time was non-destructively assessed upon weighing pots plus plants on days 12, 24,36, 48, 60 and 72 after

transplanting and then deducting pot plus soil weight. Cumulative Water Use Efficiency (WUE_{FB}) was calculated based on relative biomass growth rate increment over water transpired (Hunter et al. 2018) by the whole plant canopy with soil evaporation minimized as described above. Destructive plant growth assessment was conducted at the end of the experiment. The harvested plants were separated into shoot and root portions by cutting stems at ground level. The weight of leaves that wilted and detached during cultivation is not included. Fresh and dry mass of each part were determined to constant dry weights to calculate shoot/root ratio. Roots were thoroughly rinsed clean through a 2-mm sieve with distilled water. Floating fine root material was also handpicked and weighed. Shoot and root tissues were oven dried at 60°C to constant weight and dry weight calculated. BER incidence was calculated as a proportion (%) of total of BER-affected fruit over total fruit number per plant.

Mechanical properties

Texture-profile analysis of tomato flesh was conducted using a TA-XT*plus* texture analyser (Stable Microsystems, UK). Forty-five fruits were harvested over a period of 3 weeks. Fruit of relatively uniform light red colouration and similar weight were harvested based on the **a* parameter (Bui et al. 2010) in the colourimeter (Konica-Minolta, model CR–400, Japan) range 28–32. Fruit were held overnight in the laboratory to equilibrate to room temperature (~ 20 °C) and flesh mechanical properties were then assessed from force–displacement curves (Giongo et al. 2019; Tonina et al. 2020). Penetrometer puncture and compression 'mechanical imprint' (MI) was conducted after Camps (2018). Skin was peeled off and three 1 cm diameter and 0.7 cm thickness discs excised and sectioned with a knife. The explants were taken between adjacent septa that divide the fruit into locular chambers. Once mounted on the Texture Analyser, a 2 mm diameter probe was disc-centre aligned and displacement effected at 10 mm/s from outer to inner pericarp disc explant flesh to 5 mm depth. The digital force–displacement curve was comprised of 250 data points. One hundred and thirty-five force–displacement curves were collected for the nine treatments. Three force–deformation profiles were obtained per fruit at each of proximal (viz., peduncle end), middle, and distal (viz., stylar end) explant positions (Appendix: Fig. 12). Average flesh firmness (N), resilience force (elastic deformation; N), and flesh stiffness (N mm^{-1}) were estimated from the force–displacement curves, Average firmness was the mean of forces during probe penetration of flesh to 5 mm depth. Resilience force was peak force required to puncture the flesh (N). Flesh stiffness (N mm^{-1}) measures the elastic behaviour of the tissue based on the maximum force (N) needed to puncture the flesh per tissue deformation (mm^{-1}) (Camps 2018; Giongo et al. 2019).

Experiment two: nutrients spatial distribution using micro-XFM

The second experiment was conducted in 2019 to assess for potential amelioration by Ca^{2+} of Na^{+} toxicity in conjunction with nutrient translocation to and distribution in the tomato fruit flesh. Control plants were irrigated with 6 mM Ca^{2+} without Na^{+} as 'normal' optimum Ca^{2+} supply (De Kreij et al. 1997). A higher concentration (18 mM Ca^{2+}) without Na^{+} was used to ascertain if higher Ca^{2+} supplementation would increase Ca^{2+} in distal flesh tissue. It was hypothesized that 6/16 Ca^{2+}/Na^{+} would negatively impact Ca^{2+} partitioning and distribution in the flesh. By contrast, 18 Ca^{2+}/16 Na^{+} was test for prospective amelioration by Ca^{2+} of Na^{+} uptake and distribution in the flesh.

In view of abundant solution under constant water supply regimes, water should exude and accumulate readily on the cut stem surface (Schoonover and Crim 2015; Hunter et al. 2018). Towards testing this proposition, soil water solution was analysed for nutrient concentration. Also, the root ball was extracted from the top ANOVApot®s and divided into two parts representing two positions on their vertical face as 5 cm up from the bottom of the ball float and 3 cm down from the surface. A 10 × 15 cm soil corer was plunged into the root ball at these two points to the pot centre. Its contents were transferred into the 250 mL containers. The sample volume was considered the corer volume in depth to the pot centre. After sampling all root balls, specific volumes of DI water equivalent to nine times the volume of the soil corer were added to each 250 mL container for one volume calculated for the sub-surface sample and another for the basal sample considering different distances from outer to centre of the pot. Containers were then placed on an end-over-end shaker for 30 min. Solutions and roots were duly separated on a 2 mm mesh sieve. Roots then were spun out in a domestic vegetable spinner and weighed fresh and then dry mass after drying to constant weight at 60 °C. Solution that remained after spinning was returned to the collected solution. Soil solutions collected so were analysed for Ca^{2+}, Na^{+}, K^{+}, and Mg^{2+} concentrations by Inductively Coupled Plasma (ICP-MS) atomic emission spectroscopy (Optima 7300 DV, Perkin Elmer; Wellesley, MA, USA).

X-ray fluorescence (XFM)

Micro-XFM was used to map and quantify the spatial distribution of the macronutrients Ca^{2+} and K^{+} in relation to their supply in solution. Terminal leaflet and fruit cross-section scanning was carried out at the Centre for Microscopy and Microanalysis (CMM) at The University of Queensland, St Lucia, QLD, Australia (Appendix: Fig. 13). The Iridium Ultra View Linescan Data micro-XFM analysis package had 250 mm × 250 mm scanning travel with a spot size of 25

µm full width at half maximum (FWHM). The 2D scanning micro-XFM maps of Ca^{2+} and K^+ intensities per voxel were converted to elemental mean, maximum, minimum and peak intensities using ImageJ version 1.52j software (Fig. 1C). Prior to detailed micro-XFM scans, a rapid exploratory scan was conducted to obtain a comparative image of the tomato terminal leaflet from the four different treatments. The area of 250 × 250 mm scanned in ~ 15 min.

After van der Ent et al. (2018), the second youngest fully expanded leaflet from the growing tip was harvested using a razor blade and immediately transported to the micro-XFM lab. Leaflets were mounted horizontally between two 4 mm thick Ultralene® films and stretched over a plastic holder to provide support and obviate dehydration (Fig. 1A). Three replicate leaflets were scanned per treatment to obtain the average fluorescence intensity of each defined element (Fig. 1B–D). Ten regions of interest (ROI) per sample comprising the mean elemental concentration per pixel were randomly chosen from petiole, midrib, vein, leaflet apex, leaflet blade, and leaf margin. By averaging intensities per pixel per treatment for 30 scans, Ca^{2+} concentrations were determined in each leaflet part. The monochromatic beam was focused on the sample for 16 h continuously at energy of 12.9 keV. Mean signal for the whole leaflet was calculated in addition to peak and minimum values per element nutrient (Fig. 1D, F, and G).

Detailed scans of sample fruit from all four treatments were made for Ca^{2+} and K^+. The fruits were harvested at full breaker stage based on external turning colour to pink (Choi et al. 1995). They were transported immediately to

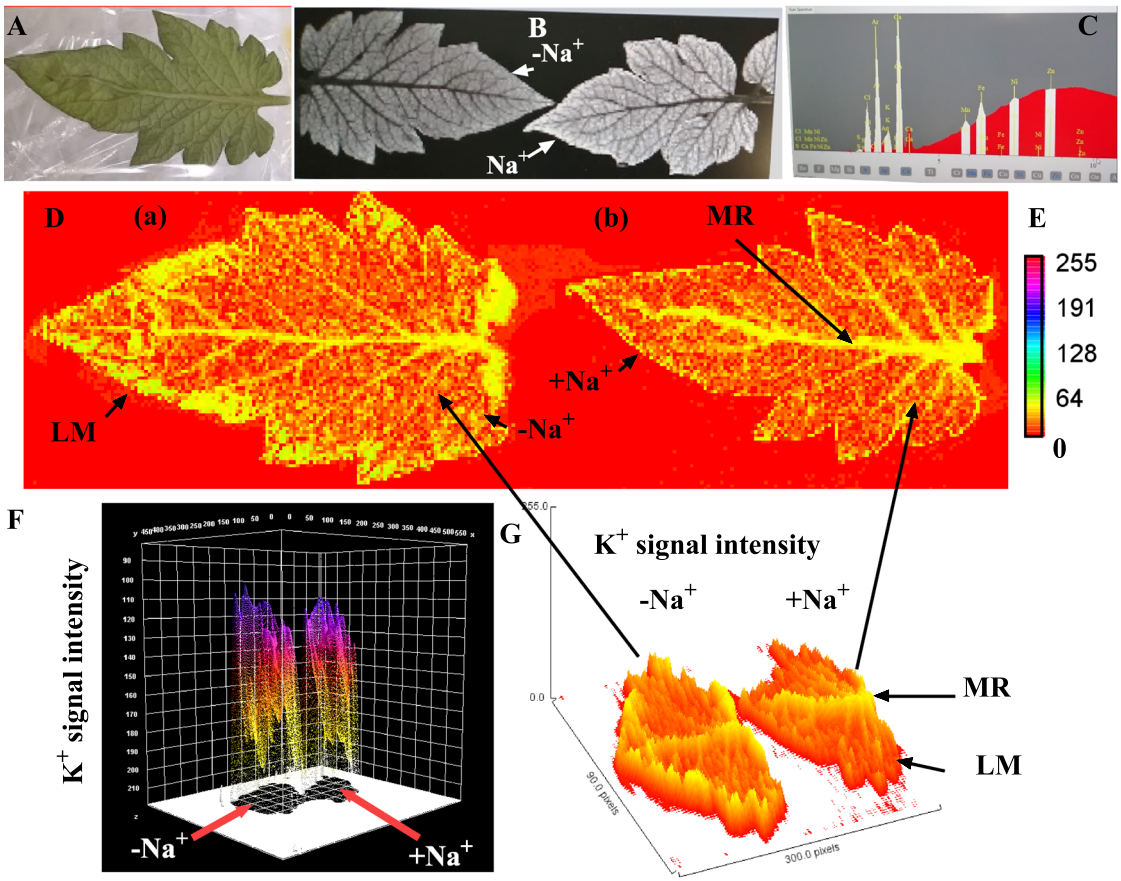

Fig. 1 XFM study protocol for tomato leaflets and fruits: **A** Leaflet sample from tomato plant mounted between two 4 mm Ultralene® films and stretched over a plastic holder to provide support and limit dehydration. **B** Scans Generated by XFM of two leaflets samples with and without Na^+ solutions. **C** Nutrient elements spatial quantification showing peaks for the tomato leaflet with 6 mM Ca^{2+} solution and no added Na^+. **D** K^+ elemental maps for control **a** 6 mM Ca^{2+} with no added Na^+ and **b** 6 mM Ca^{2+}/16 mM Na^+ for tomato leaf terminal leaflet. Each map is false coloured to help visualize K^+ distribution patterns. **E** The pseudo-colour bar indicates relative intensity for K^+ distribution maps of tomato leaflets. Higher intensities correspond to higher K^+ contents. **F** 3D surface plots of K^+ intensity histograms of two tomato leaflets with and without Na^+ solution. Histograms were generated for all voxels in the leaflet images. **G** Surface plots showing spatial K^+ signal intensity distribution in two tomato leaflets: – Na^+; no added Na^+, and + Na^+; 16 mM Na^+. MR; mid rib, LM; leaflet margins

the micro-XFM lab and prepared ~ 1 h before scanning to minimize any potential dehydration. The fruit were cut into two halves from proximal to the distal ends. Thin (5 mm) uniform pericarp slices were cut with razor by hand and used to map longitudinal nutrient distribution and concentrations. Also, longitudinal 5 mm slices from the proximal and distal tissues and including skin were obtained from the external abaxial to the internal adaxial side of the fruit. The slices were mounted between the two 4-mm Ultralene® films stretched over the tomato slices sample holder. The fruit samples were then scanned using 12 keV excitation energy beam in a raster pattern to create Ca^{2+} and K^{+} intensity maps of fluorescent x-rays emitted from the fruit. Scanning was 20 h for 700 µm pixel. Fluorescence signal intensities for the elements were calculated with ImageJ version 1.52j software. ROI analysis of interrogated points was carried out to assess variation in elemental concentrations across fruit sections from exocarp to locular cavity. A total of 30 ROI per treatment were randomly chosen per each tissue type.

Inductively coupled plasma mass spectrometry (ICP-MS)

Tomato flesh mineral analysis was performed at the end of experiment towards quantifying 'Roma' flesh nutrient concentration in response to various treatments; 6 mM Ca^{2+} and no Na^{+}, control; 6 mM Ca^{2+} and 16 mM Na^{+}; 18 mM Ca^{2+} and no Na^{+}; 18 mM Ca^{2+} and 16 mM Na^{+}.

Briefly, two representative fully ripened fruits of similar size were harvested from 12 plants, three per treatment, and carefully washed with deionized water. Fruit skin was removed with a sharp knife and oven-dried at 70 °C to constant weight. Dried flesh samples were finely ground by mortar and pestle and 300 mg dry weight was used for analysis. Samples were wet digested with nitric acid (HNO_3) at 140 ˚C for 5 min followed by increase to 210 ˚C over 10 min, holding at 210 ˚C for 10 min, and cooling for 10 min. Resultant solutions were diluted with 35 ml deionized water and analysed by ICP-MS.

Data analysis

Each treatment consisted of three replicates and results are expressed on a dry weight basis. All ICP-MS data were analysed using by two- or multi- variate ANOVA program. Differences between means were considered significant at $p < 0.05$. AOV was performed in Minitab® v. 19 (Minitab Inc., State College, PA, USA) and $p < 0.05$ was again considered significant. The post hoc Tukey test at the 5% level of significance ($\alpha = 0.05$) was applied for differences between means. Linear and non-linear regression analyses were performed using GraphPad Prism version 8.0.0 (San Diego, California USA). Graphed data were expressed as mean ± standard. Linear regression analyses were denoted "ns" when not significant ($p > 0.05$) or with asterisks (*, **, ***) when significant ($p < 0.05$, $p < 0.01$, and $p < 0.001$, respectively).

Results

Experiment one: nutrients and mechanical properties

Plant growth, water loss and WUE

Pants had steady daily water uptake during their first 2 weeks of growth (Fig. 2). Uptake dropped once Na^{+} imposition commenced. The fall began slowly for 32 mM Na^{+} solution and then dropped sharply at 2 weeks after salt stress imposition at the vegetative stage preceding the flowering stage. This fall was associated with a decrease in growth rate compared to Na^{+} free irrigation solution. Highest daily uptake was 2200 ml $plant^{-1}$ with the highest Ca^{2+} no Na^{+} treatment. Lowest uptake was 200 ml $plant^{-1}$ under the highest Na^{+} supply regime. Daily water consumption increased over time in the absence of Na^{+} in the solution treatments (Fig. 2).

Plant fresh mass at 72 days was linearly related ($R^2 = 0.92$) to total water uptake (Fig. 3). There were significant $Ca^{2+} \times Na^{+}$ interactions (Tukey's test; $p < 0.05$) for average daily water uptake (ml day^{-1}) and consumption (ml $plant^{-1}$) (Table 1). Irrigation with 16 mM Na^{+} solution brought about a 475 ml or 41% drop in average daily transpiration water consumption. The 32 mM solution induced a greater, namely 615.6 ml or 53%, drop. The 18 mM Ca^{2+} irrigation solution was associated with significantly increased daily overall water consumption compared to 12 mM Ca^{2+} (Table 1).

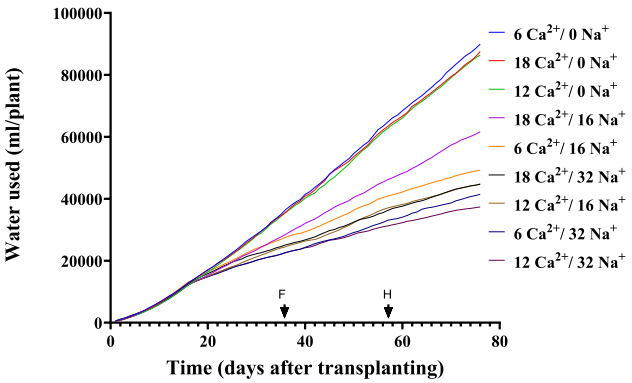

Fig. 2 Cumulative daily water loss (ml $plant^{-1}$) for 'Roma' tomato plants s grown with different Ca^{2+} and $Na.^{+}$ solutions on a constant water table over 76 days. F; initiation of flowering, H; initiation of fruit harvest. $N = 5$

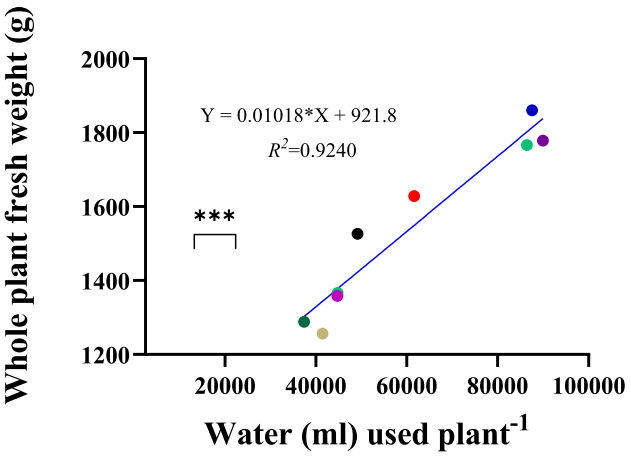

Fig. 3 Linear relationship between harvested 'Roma' tomato plant biomass (fw.plant–^{1}) and water consumption ml.plant^{-1} over the 76 d growth period. The plants were grown under different calcium and sodium concentrations

Serial addition of Na^+ via irrigation solution caused progressive deterioration for all plant growth parameters (Tukey's test; $p < 0.01$) over the time course of the experiment. There was a distinct drop in plant biomass increments upon Na^+ application. Compared to no added Na^+, introduction of 16 mM Na reduced total plant biomass by 252 g corresponding to 14% reduction. The 32 mM Na^+ solution resulted in a more significant decline in biomass of 539 g compared to no added Na^+, this being a 30% reduction (Table 1). At 16 mM Na^+ in nutrient solution, shoot biomass was reduced 205 g or 21.3%, and at 32 mM Na^+ the decrement was 348 g or 36.2%. However, increasing Ca^{2+} from 6 to 18 mM restored shoot biomass with a 22% increase in total fresh biomass under 32 mM Na^+. Lower Ca^{2+} rates had no such ameliorative effect for fresh shoot biomass. Root fresh weight dropped by 140 g or 16.5% under 32 mM Na^+ compared to no added Na^+ solution (Table 1). Table 1 shows that mean tomato fruit weight was significantly reduced by 16- and 32-mM Na^+ irrigation solutions, while Ca^{2+} had no effect. The 16- and 32-mM Na^+ irrigation treatments caused 30 and 43.2% increases in BER, respectively. Although BER% dropped significantly with increasing Ca^{2+} supply, it was still found in 24% of fruit that received high Ca^{2+}/Na^+ (Table 1).

Fruit mechanical properties

Ca^{2+} and Na^+ supply effects on mechanical properties of tomato flesh were assessed as average flesh firmness (N), peak flesh puncture resistance force (N) and flesh stiffness (N mm^{-1}) (Table 2). Proximal tissue was firmer regardless of Ca^{2+}/Na^+ ratios than were middle and distal tissues. Irrigation with saline solution markedly reduced average flesh firmness (Table 2). Force–displacement curves showed that flesh stiffness (N mm^{-1}) enhancement was not proportional to Ca^{2+} supply. Increasing Ca^{2+} from 6 to 12 mM enhanced flesh stiffness by 9.8%. Further increase of Ca^{2+} to 18 mM increased flesh stiffness by 24.9%. In contrast, salinity induced a drop in flesh stiffness. Under 16 mM Na^+ solution, raising Ca^{2+} levels to 18 mM restored flesh stiffness by 35.4% in all flesh tissues. However, with an increase of Na^+ to 32 mM, supplemental Ca^{2+} (18 mM) had no effect. Proximal tissues were markedly stiffer than middle and distal tissues (Table 2).

The peak force to puncture flesh dropped by 48.1% as Na^+ was increased from 0 to 16 mM (Table 2). It further dropped by 64% at 32 mM Na^+. Conversely, the maximum compression force to penetrate tomato fruit flesh was significantly (Tukey's test; $p < 0.05$) higher at 18 mM Ca^{2+} supply by 22% and 21.6% as compared to 12 and 6 mM Ca^{2+}, respectively. Moreover, there was a notable drop in peak penetration force from proximal to the middle and distal tissues by 44.5% irrespective of the Ca^{2+}/Na^+ supply ratio. Overall, Ca^{2+}/Na^+ interaction presented in Table 2 showed that Ca^{2+} was ineffective to restore flesh stiffness and peak force caused by added Na^+. However, Ca^{2+} restored flesh firmness ($p < 0.05$) and substantially reduced the flesh softening observed with the added Na^+ treatment.

Fruit mineral nutrients ICP-MS

Nutrients in different flesh tissues were influenced by Ca^{2+} and Na^+ supply and their interaction (Table 3). Increasing Ca^{2+} in the irrigation solution from 6 to 18 mM increased fruit Ca^{2+} by 30% and decreased Na^+ by up to 44% but had no effect on fruit K^+. While the Ca^{2+}-enhanced solution showed increased Ca^{2+} in the tomato flesh when compared to controls, other nutrients, particularly Mg^{2+} were also increased in the tomato flesh. Similarly, an increase to 16 mM Na^+ resulted in a ninefold increase in Na^+ concentration and a decrease of Ca^{2+}, K^+ and Mg^{2+} by up to 36%, 11% and 17%, respectively.

Ca^{2+} concentration was higher in proximal tissues by 1.8-fold and 2.7-fold over than that in middle and distal tissues, respectively (Table 3). Unlike for Ca^{2+}, concentrations of K^+, P, and, to a lesser extent, Mg^{2+} displayed a gradient increase from proximal to distal tissues. In contrast, concentrations of Na^+ in fruit tissues remained relatively constant (Table 3).

Na^+ supply reduced Ca^{2+} and K^+ concentrations in all flesh tissues (Table 3). Ca^{2+} supply enhanced its levels in proximal and middle mesocarp tissue but had little effect in distal tissues (Table 4). Even with distilled water, a small amount of Na^+ was detected in the solution, despite the absence of added Na^+. It is likely that Na^+ originated from the medium. The washed sand exhibited an electrical conductivity of 1.2 ds/m, along with other nutrients, including

Table 1 Mean vegetative, physiological, water uptake and blossom end-rot levels. The plants were grown under different (Ca^{2+}; 6, 12 and 18 mM) and sodium (Na^{+}; 0, 16, 32 mM) concentrations

Tomato	*n*	Plant biomass (g)	Shoot biomass (g)	Root biomass (g)	Root/shoot	Fruit weight (g)	Fruit dry matter (g)	Fruit set number/plant	Water consumption (mL/plant)	Average daily water uptake (mL/day)	BER %
Ca^{2+} supply											
6 mM	15	1538 a	738 a	767 a	1.12 a	34.8 a	2.79 a	33 a	60,191 ab	792 ab	35.1 a
12 mM	15	1512 a	742 a	791 a	1.12 a	37.4 a	3.19 a	31 a	56,201 b	739 b	30 ab
18 mM	15	1618 a	852 a	808 a	0.97 a	40.7 a	3.64 a	34 a	64,647 a	851 a	24 b
Na^{+} supply											
0	15	1820 a	962 a	851 a	0.89 b	72.9 a	5 a	34 a	87,979 a	1158 a	15.9 c
16 mM	15	1568 b	757 b	804 a	1.1 a	20.7 b	2.28 b	26 a	51,871 b	683 b	30.1 b
32 mM	15	1281 c	614 c	711 b	1.22 a	19.3 b	2.34 b	25 a	41,190 c	542 c	43.2 a
P values											
Ca^{2+} level (A)		NS	NS	NS	NS	NS	NS	NS	***	***	*
Na^{+} level (B)		***	***	**	**	***	***	NS	***	***	***
A × B		NS	NS	NS	NS	NS	NS	NS	*	*	NS

Means followed by the same letter are not statistically significant (Tukey's Test, $p < 0.05$) and *, **, ***, and "NS" indicate significant differences at $p < 0.05$, $p < 0.01$, $p < 0.001$, and non-significant differences, respectively.

Table 2 Effects of calcium (Ca^{2+}; 6, 12 and 18 mM) and sodium (Na^+; 0, 16, 32 mM) in irrigation water on 'Roma' tomato average flesh firmness, peak force (N) and flesh stiffness (N mm^{-1}). Proximal, middle and distal flesh was assessed using a force digital force–displacement meter. Interactions for $Ca^{2+} \times Na^+$ are reported for 76 days after imposition of saline irrigation water treatments

Tomato flesh mechanical properties	*n*	Flesh firmness (N)	Peak force (N)	Flesh stiffness
Ca^{2+} supply				
6	15	0.5 b	0.85 b	0.22 b
12	15	0.52 b	0.84 b	0.28 ab
18	15	0.63 a	1.08 a	0.29 a
Na^+ supply				
0	15	0.89 a	1.48 a	0.37 a
16	15	0.44 b	0.77 b	0.22 b
32	15	0.32 c	0.53 c	0.16 b
Fruit section				
Proximal	15	0.77 a	1.32 a	0.32 a
Middle	15	0.45 b	0.73 b	0.23 b
Distal	15	0.43 b	0.72 b	0.2 b
P values				
Ca^{2+} level (A)		*	**	*
Na^+ level (B)		***	***	***
Fruit section (C)		***	***	***
A × B		*	NS	NS
B × C		***	***	*

Means followed by the same letter are not statistically significant (Tukey's Test, $p < 0.05$) and *, **, ***, and "NS" indicate significant differences at $p < 0.05$, $p < 0.01$, $p < 0.001$, and non-significant differences, respectively.

Na^+ (0.22 cmol +/kg), Ca^{2+} (7.5 cmol +/kg), and chloride (15 mg/kg) (Table 4). Ca^{2+} supply reduced Na^+ concentrations in middle and distal tissues but had no effect on K^+ concentration in these tissues. Increasing Ca^{2+} concentration in irrigation solution to 18 mM showed an interaction between Ca^{2+} and Na^+ with decreased Na^+ concentrations of 44.4%, 60.4% and 35.2% in proximal, middle and distal tissues, respectively.

This experiment confirmed limited translocation of Ca^{2+} (Tukey's test; $p < 0.001$) to fruits compared to the leaves despite the relatively high VPD conditions (0.9–2.4 kPa) that prevailed (Fig. 4). There were no significant differences in the Mg^{2+}, K^+ and Na^+ accumulation and translocation between leaves and fruits (Fig. 4).

Experiment two: nutrients spatial distribution using micro-XFM

A homogenous distribution of nutrients in the sand-Perlite growing medium profile was sought from the constant water table ANOVApot® culture system. This proposition was based on a constant and progressive water and nutrients movement to the soil profile. To test this, the spatial heterogeneity of the nutrients from different depths within pots was characterized. Results showed the spatial distribution of all nutrients tested in the soil profile was homogenous, except for Na^+. Na^+ tended to accumulate in the upper profile (Fig. 5).

Concentrations of Ca^{2+} and Na^+ in the growing media were directly related to concentrations applied in the irrigation solutions. Increasing Ca^{2+} from 6 to 18 mM increased Ca^{2+} in the soil solution by nearly threefold (Fig. 5A). Concentrations of Ca^{2+} in the growing medium solution ranged from 36 mg l^{-1} in the bottom of pots for 6 Ca^{2+}/16 Na^+ irrigation solution to 373 mg l^{-1} in the bottom of pots with 18 Ca^{2+}/16 Na^+ solutions (Fig. 5A). Similarly, increasing Na^+ in irrigation solution from 0 to 16 increased Na^+ in the growing medium solution by ~ fourfold (Tukey's test; $p < 0.001$) with no changes in media solution concentrations of Ca^{2+} being found (Fig. 5B). Increased Ca^{2+} or Na^+ supply had no effect on K^+ concentration in the top and bottom of the media profile (Fig. 5C). Increased Ca^{2+} in the solution from 6 to 18 mM reduced sodium adsorption ratio (SAR) by over 54%. Increased Na^+ in solution from no added Na^+ to 16 mM increased SAR by 82% (Fig. 5D). Unlike Na^+, SAR values were stable down the growing media profile (Fig. 5D).

Leaflet XFM

Fluorescence intensity in whole leaflet scans showed mean peaks for Ca^{2+} being spatially high in the leaflet blade between veins and leaflet tips (Fig. 6A). K^+ was relatively high in the leaflet midrib and veins (Fig. 6B). Micro-XFM showed Ca^{2+} in the leaflet had been translocated towards the margin. K^+-rich areas in the midrib and near veins corresponded inversely with low Ca^{2+}. The distribution of Ca^{2+} concentrations generally trended in the order: leaflet apex > leaflet margins > leaflet blade > veins > midrib > petiole (Table 5).

There was marked variation in relative Ca^{2+} concentrations across the tomato terminal leaflets in response to different $Ca^{2+}$and Na^+ concentrations in the irrigation solution (Fig. 6A). Increasing Ca^{2+} from 6 to 18 mM increased the Ca^{2+} signal by 40.6% (Table 5). In whole leaflet scanning, 16 mM Na^+ evidently reduced Ca^{2+} signal intensity by 35.6% compared to no added Na^+ (Table 5). A strong interaction (Tukey's Test, $p < 0.0001$) between Ca^{2+} and Na^+ was found for Ca^{2+} signal of the whole leaflet. High Ca^{2+} ameliorated Na^+, as evidenced by the restoration of the overall signal intensity in the terminal leaflet following the addition of Ca^{2+}. (Table 5). Peak Ca^{2+} signal was found with the highest Ca^{2+} and no Na^+ treatment (Fig. 7A). Interactions reflected that applying 16 mM Na^+ in nutrient solution reduced

Table 3 Nutrient concentrations of 'Roma' tomato flesh in response to different levels of calcium (Ca^{2+}; 6 and 18 mM) and sodium (Na^{+}; 0, 16 mM) in irrigation water

Treatments	*n*	Nutrients concentration of tomato flesh without skin				
		Ca^{2+} (g/Kg)	Na^{+} (g/Kg)	K^{+} (g/Kg)	P (g/Kg)	Mg^{2+} (g/Kg)
Ca^{2+} levels						
6 mM	18	0.64 b	2.66 a	25.36 a	3.09 a	1.11 b
18 mM	18	0.91 a	1.48 b	26.17 a	2.89 b	1.18 a
Na^{+} level						
0	18	0.95 a	0.41 b	27.36 a	3.05 a	1.25 a
16 mM	18	0.6 b	3.73 a	24.18 b	2.94 a	1.04 b
Tissue type						
Proximal	12	1.21 a	2.44 a	22.63 c	2.54 c	1.03 b
Middle	12	0.67 b	1.97 a	25.01 b	2.99 b	1.13 b
Distal	12	0.45 c	1.8 a	29.68 a	3.44 a	1.26 a
P values						
Ca^{2+} level (A)		***	**	NS	*	*
Na^{+} level (B)		***	***	***	NS	***
Fruit section (C)		***	NS	***	***	***
A × B		*	**	NS	*	NS
A × C		**	NS	NS	NS	NS
A × B × C		*	NS	NS	*	NS

Means followed by the same letter are not statistically significant (Tukey's Test, $p < 0.05$) and *, **, ***, and "NS" indicate significant differences at $p < 0.05$, $p < 0.01$, $p < 0.001$, and non-significant differences, respectively.

Table 4 Nutrient concentrations in tomato 'Roma' flesh in relation to different levels of calcium (Ca^{2+}; 6 and 18 mM) and sodium (Na^{+}; 0 and 16 mM) supply in irrigation solution. The means presented are for different flesh tissue, viz., proximal, middle, and distal

Fruit tissues										
Tomato flesh nutrients concentration	*n*	Proximal			Middle			Distal		
		Ca^{2+} (g/Kg)	Na^{+} (g/Kg)	K^{+} (g/Kg)	Ca^{2+} (g/Kg)	Na^{+} (g/Kg)	K^{+} (g/Kg)	Ca^{2+} (g/Kg)	Na^{+} (g/Kg)	K^{+} (g/Kg)
Ca^{2+} levels										
6 mM	6	0.97 b	3.07 a	22.67 a	0.51 b	2.74 a	24.11 a	0.45 a	2.17 a	29. 3 a
18 mM	6	1.45 a	1.8 a	22.58 a	0.83 a	1.21 b	25.9 a	0.45 a	1.42 b	30 a
Na^{+} level										
0	6	1.47 a	0.36 b	24.24 a	0.82 a	0.37 b	26.35 a	0.56 a	0.5 b	31.5 a
16 mM	6	0.94 b	4.52 a	21.01 b	0.52 b	3.58 a	23.66 b	0.34 b	3.09 a	27.9 b
Ca^{2+} × Na^{+} interaction										
6 × 0	3	1.38 a	0.33 b	23.25 ab	0.65 b	0.36 b	26.09 a	0.58 a	0.58 c	30.7 a
6 × 16	3	0.55 b	5.81 a	22.09 ab	0.38 c	5.13 a	22.14 a	0.32 a	3.75 a	27.9 a
18 × 0	3	1.55 a	0.38 b	25.24 a	0.99 a	0.38 b	26.62 a	0.54 a	0.41 c	32.3 a
18 × 16	3	1.34 a	3.22 ab	19.93 b	0.66 b	2.03 b	25.18 a	0.35 a	2.43 b	27.8 a
P values										
Ca^{2+} level (A)		**	NS	NS	***	*	NS	NS	**	NS
Na^{+} level (B)		**	***	**	***	***	*	*	***	*
A × B		*	*	*	NS	*	NS	NS	*	NS

Means followed by the same letter are not statistically significant (Tukey's Test, $p < 0.05$) and *, **, ***, and "NS" indicate significant differences at $p < 0.05$, $p < 0.01$, $p < 0.001$, and non-significant differences, respectively.

Ca^{2+} mean signal by over 59.8% compared to the control (Fig. 7B). Such effects of added Ca^{2+} restored mean signal values (Fig. 7D; Table 5).

Under 16 mM Na^{+} solution, K^{+} concentrations in different leaf parts dropped notably (Fig. 6B). Leaflet XFM scans revealed higher K^{+} accumulation in midrib and veins

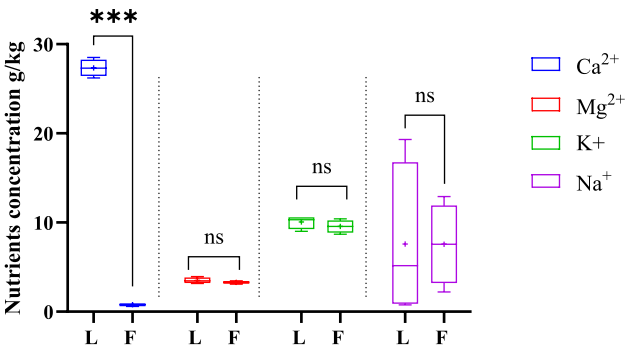

Fig. 4 Nutrients concentration for 'Roma' tomato fruit (F) and leaves (L) from plant irrigated with varying calcium (Ca^{2+}; 6 and 18 mM) and sodium ($Na.^{+}$; 0 and 16 mM) solutions on a constant water table. *, **, *** and "ns" indicate significant differences at $p < 0.05$, $p < 0.01$, $p < 0.001$, and non-significant differences, respectively. $N = 3$

as Ca^{2+} supply was increased from 6 to 18 mM in irrigation solution (Fig. 6B).

Fruit micro-XFM

Micro-XFM signals in fruit were weaker than in leaves such that exposure time was extended from 16 to 20 h. The scan showed relatively high Ca^{2+} signal for Ca^{2+}-enhanced irrigation solutions. Average fruit Ca^{2+} signal intensity was 22.5% greater with increased Ca^{2+} in the irrigation solution. With low Ca^{2+} supply, Ca^{2+} 'hotspots' were evident as pinkish areas in exocarp tissue. Higher Ca^{2+} supply increased Ca^{2+} in the mesocarp (Fig. 8A). Ca^{2+} signal reflecting concentration in the exocarp was up to ~twofold higher than in the mesocarp (Table 6). K^{+} was distributed throughout the outer pericarp near the exocarp (Fig. 8B). In contrast to leaflet tissue, K^{+} intensity was twofold higher than Ca^{2+} in fruit tissues. Strongest Ca^{2+} signal was observed in exocarp tissue and weakest expectedly in the locular cavity (Table 7).

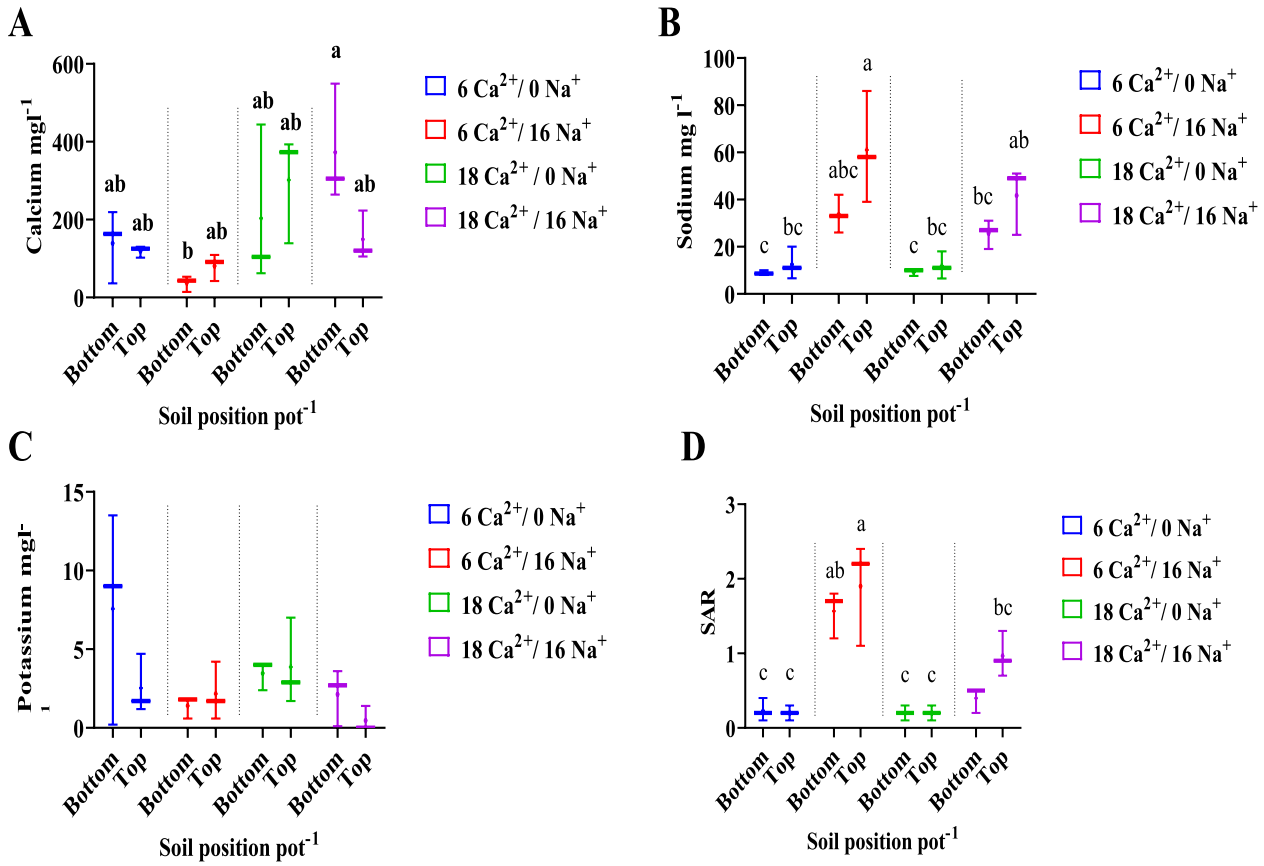

Fig. 5 Interaction plots between for calcium (Ca^{2+}: 6, 18 mM) and sodium (Na^{+}: 0, 16 mM) in solution and sand growing medium layer (lower, top) in pot for Ca^{2+} (**A**), Na^{+} (**B**), and $K.^{+}$ (**C**) and sodium adsorption ratio (SAR; **D**) spatial distribution in soil solution over a constant water table at 74 days after treatments imposition. Different letters associated with means indicate significant differences among treatments by Tukey's test ($p < 0.05$). An absence of letters indicates no significant difference among treatments. Values are means of five replicate samples. Boxes represent the interquartile ranges, whiskers extend to the 10% and 90% percentiles, respectively. $N = 3$

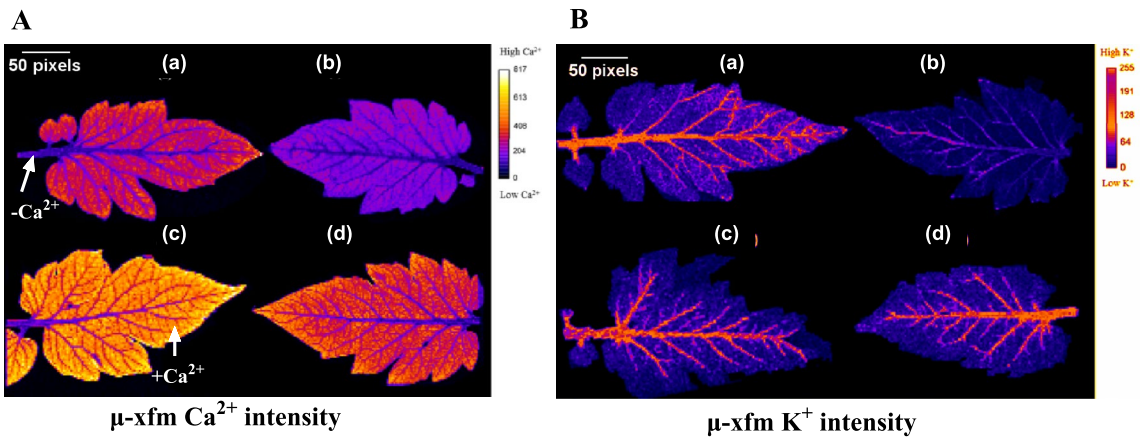

Fig. 6 Micro-XFM element maps showing spatial distribution patterns for Ca^{2+} (**A**) and K^+ (**B**) in 'Roma' tomato terminal leaflets. The sampled leaflets were selected from the last fully growing leaves. The plants received calcium (Ca^{2+}; 6 and 18 mM) and sodium (Na^+; 0 and 16 mM) in irrigation solution. a, b, c, and d represent 6 mM Ca^{2+}/no Na^+, 6 mM Ca^{2+}/16 mM Na^+ mM, 18 mM Ca^{2+}/no Na^+ mM, and 18 mM Ca^{2+}/16 mM Na^+ mM treatments for Ca^{2+} (**A**) and K^+ (**B**) scans, respectively. The pseudo-colour maps help visualize the spatial distribution patterns of Ca^{2+} and K^+. The original grayscale 8-bit maps were pseudo-coloured with a fire look-up table LUT (http://fiji.sc/). Colour range black (lowest signal) to white (brightest signal) for Ca^{2+} and black (lowest signal) to red for K^+ (brightest signal) reflecting concentration of the lowest and the highest signal intensity obtained as shown in colour scale bar. $+Ca^{2+}$; high Ca^{2+} signal, $-Ca^{2+}$; low $Ca.^{2+}$ signal. $N=3$

Table 5 Micro-XFM calcium signal intensity of various tomato terminal leaflet parts in response to different levels of calcium (Ca^{2+}; 6 and 18 mM) and sodium (Na^+; 0 and 16 mM) in irrigation solution. Each replicate is the average of 45 region of interest (ROI) on specific leaflets

Treatments	Tomato terminal leaflet parts signal intensity						
	Petiolule (rachis)	Mid rib	Veins	Leaflet blade (centre)	Leaflet margins	Apex	Leaflet total
Ca^{2+} supply							
6 mM	147.3 a	141 b	172 b	366 b	435 b	579 b	235 b
18 mM	140.7 a	185 a	208 a	590 a	623 a	695 a	395 a
Na^+ supply							
0	149.5 a	172 a	224 a	519 a	624 a	681 a	383 a
16 mM	138.5 a	154 a	155 b	437 a	434 b	594 a	246 b
P values							
Ca^{2+} level (A)	NS	***	**	**	***	*	***
Na^+ level (B)	NS	NS	***	NS	***	NS	***
A × B	NS	NS	NS	NS	NS	NS	***

Means followed by the same letter are not statistically significant (Tukey's Test, $p < 0.05$) and *, **, ***, and "NS" indicate significant differences at $p < 0.05$, $p < 0.01$, $p < 0.001$, and non-significant differences, respectively.

Longitudinal elemental mapping from proximal to distal tissues showed that Ca^{2+} accumulated in 'hot spots' in proximal tissues (Fig. 9A). Consistent with ICP-MS analysis, micro-XFM image data showed increased in Ca^{2+} in proximal and middle mesocarp fruit tissues when the irrigation solution was Ca^2-enhanced. This response was relatively minor in distal fruit tissue, with only 18.5% localized in the exocarp and 17.4% in the mesocarp in relation to other tissue types (Table 6).

Peak localized Ca^{2+} increased by over threefold as Ca^{2+} increased from 6 to 18 mM (Table 7). The greatest Ca^{2+} signal peak was with 18 mM Ca^{2+}/16 mM Na^+ treatment at over 255 µm/pixel (Fig. 10A). The maximum leaflet signal intensity was 3-times higher than fruit with nearly 800 µm/pixel. An increase to 16 mM Na^+ reduced fruit Ca^{2+} maximum signal and septa concentration by 9.3 and 20.4%, respectively, while remaining unchanged in other tissues (Table 7). The Ca^{2+}-enhanced solution increased the overall Ca^{2+} concentration by threefold from proximal to distal. These results were very comparable to the Ca^{2+}-enhanced solution and no Na^+.

The utilization of micro-XFM allowed for rational comparison between Ca^{2+} concentrations in BER tissues and the surrounding healthy tissues. Micro-XFM analysis revealed

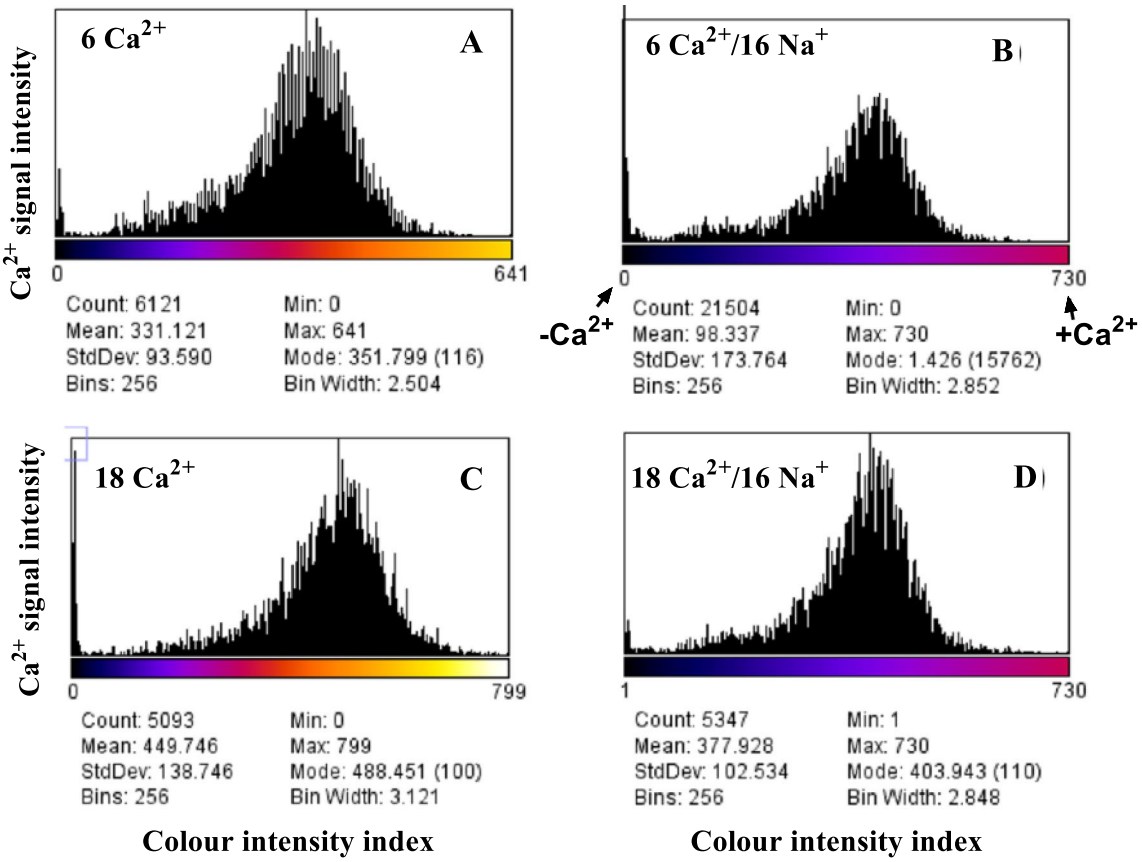

Fig. 7 Micro-XFM calcium scans of tomato terminal leaflets of most recently expanded leaf harvested from individual plants grown on **A** 6 mM Ca^{2+}, **B** 6/16 Ca^{2+}/Na^{+}, **C** 18 Ca^{2+}, and **D** 18/16 Ca^{2+}/Na^{+} irrigation solution treatments. Count is number of cells. Mean is the mean value. StdDev is the standard deviation. The Min and Max refer to the lowest and highest values of bins, respectively Bins is the number of the bins. Bin width is the width of each bin within the histogram. Histograms show relative count, mean, peak, minimum Ca^{2+} signal intensity after treatments imposed for 74 days. $+Ca^{2+}$; highest Ca^{2+} signal, $-Ca^{2+}$; lowest Ca.$^{2+}$ signal per treatment. $N=3$

that Ca^{2+} in the BER tissue was up to 4-folds higher than in the surrounding sound tissues (Fig. 9B).

Added Na^{+} (16 mM) resulted in a significant decrease in K^{+} (Fig. 11B). Added Ca^{2+} partially ameliorated Na^{+} toxicity through increasing K^{+} in the fruit exocarp (Fig. 8B), but had little effect on the mesocarp and fruit as a whole (Fig. 11A).

Discussion

Water uptake

Ca^{2+} can be involved in plant salt tolerance and water relations (Tuna et al. 2007; Hocking et al. 2016; Feng et al. 2018). In the present study, interactive effects of Ca^{2+} and Na^{+} on plant daily water uptake was assessed. Bu employing a 'Twinpot Management System' for maintaining a constant water table (Hunter and Scattini 2014), non-invasive continuous assessment of WUE was based on cumulative weight gain per unit water transpired per plant. Previous research has indicated that reduction in irrigation amounts potentially enhance plant WUE for a slight drop in biomass and yield. Consistent with Reina-Sánchez et al. (2005), tomato plants irrigated with Na^{+} solution in this study transpired over 50% less water, thereby resulting in increased WUE. These findings correspond to Wan et al. (2007) and Lovelli et al. (2012), but contradict Yang et al. (2019) who found that WUE was inversely correlated with salinity. A strong relationship between final harvested plant weight and water consumed per plant in the present study reflects gain in WUE. Vegetative losses were mitigated when Ca^{2+} was added to the nutrient solution, particularly under low saline regime. These observations corroborate results of Tuna et al. (2007). The present study determined a strong downtrend in WUE, particularly over the first 48 days. This concurs with Molina-Montenegro et al. (2020) who demonstrated a drop in WUE on days 30, 60, and 100 with both saline and non-saline conditions in tomato plants.

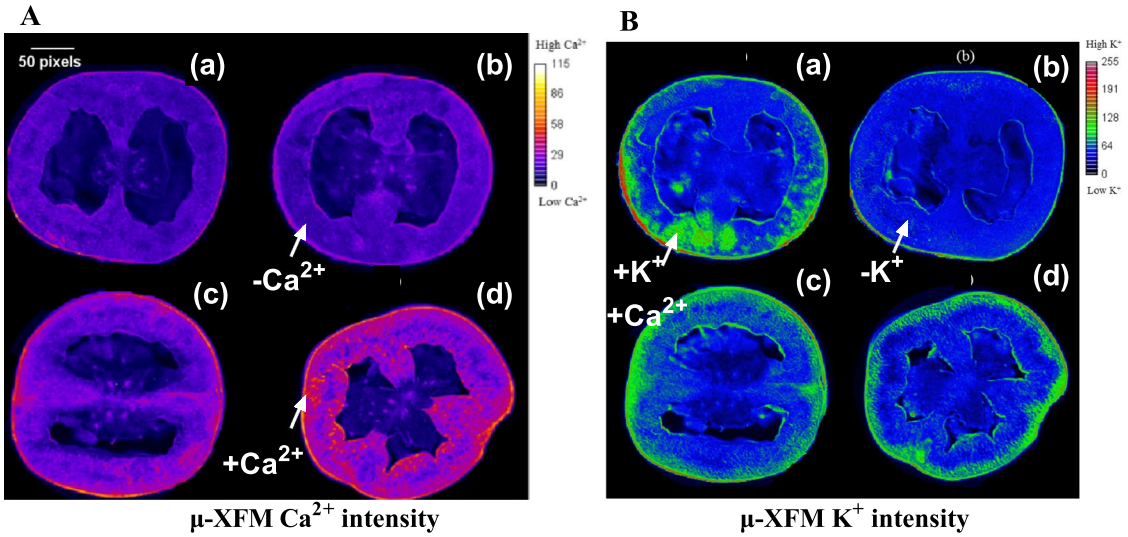

Fig. 8 X -ray fluorescence microscopy element maps map showing spatial distribution patterns of calcium (**A**) and potassium (**B**) in the proximal tissue of breaker stage 'Roma' tomato fruit. Plants received different amounts of calcium (Ca^{2+}; 6 and 18 mM) and sodium (Na^{+}; 0 and 16 mM) in irrigation solution. The letters a, b, c, and d correspond to 6 Ca^{2+}/16 Na^{+} mM, 6 mM Ca^{2+}/no Na^{+}, 18 Ca^{2+}/16 mM Na^{+} and 18 Ca^{2+}/no Na^{+} treatments for **A** (Ca^{2+}) and **B** (K^{+}) scans, respectively. Micro-XFM signal intensity (concentration) is shown as a pseudo-colour scale. The original grayscale 8-bit maps were pseudo-coloured with a rainbow look-up table (LUT). Colour ranges from black (lowest signal) to white (brightest signal) for Ca^{2+} and black (lowest signal) to red for $K.^{+}$ (brightest signal) are shown in the colour scale bars. *N* = *3*

Table 6 Calcium micro-XFM elemental analysis (μm/pixel) of various tomato exocarp and mesocarp tissues of tomato fruit in response to different levels of calcium (Ca^{2+}; 6 and 18 mM) and sodium (Na^{+}; 0 and 16 mM) in irrigation solution

Tomato	*n*	Exocarp	Mesocarp
Ca^{2+} supply (A)			
6 mM	18	79 b	36.9 b
18 mM	18	139 a	74.3 a
Na^{+} level (B)			
0	18	112 a	58 a
16 mM	18	105 a	53.3 a
Tissue (C)			
Proximal	12	155 a	82.3 a
Middle	12	111 b	55.5 b
Distal	12	60 c	29 c
P values			
Ca^{2+} level (A)		***	***
Na^{+} level (B)		NS	NS
Tissue (C)		***	***
A × B		***	*
A × C		***	***
B × C		***	NS

Means followed by the same letter are not statistically significant (Tukey's Test, $p < 0.05$) and *, **, ***, and "NS" indicate significant differences at $p < 0.05$, $p < 0.01$, $p < 0.001$, and non-significant differences, respectively.

Average daily water consumption increased when Ca^{2+} was added to the saline nutrition solution (Table 1). Ca^{2+} is vital in the water transport of plants growing under salt stress. Ca^{2+} concentration in the nutrient solution determines the restoration of root hydraulic conductivity (Navarro et al. 2000). Tuna et al. (2007) reported that a Ca^{2+} beneficial effect on root hydraulic conductivity mitigates the deleterious effect of salinity on water uptake). Consistent with this investigation, increasing Ca^{2+} in soil solution to ˃10.0 mM has been shown to reduce Na^{+} toxicity in various plant species (e.g., Cramer 2002; Tuna et al. 2007; Tattini and Traversi 2009).

Low and uneven soil moisture in the media may reduce mass flow and nutrient diffusion via the soil solution (Prieto et al. 2012), thereby limiting plant nutrient uptake. Plants proliferate roots in regions where nutrients and water are most available (Day et al. 2003). Root selectivity towards nutrient-rich patches may limit plant growth by changing both the amount of root proliferation and the distance that roots travel in media with uneven moisture distribution (McNickle et al. 2016). The ANOVApot® system was employed in this study towards homogenous vertical moisture distribution in the media and towards even distribution of nutrients. However, Na^{+} distribution patterns showed a tendency to accumulated (> 39%) in the upper region of the profile (Fig. 5). Previous studies show that Na^{+} has strong migration ability upwards along with capillary water movement (Perelman et al. 2020). As water evaporates at

Table 7 Interactions between Ca^{2+} and Na^{+} in irrigation solution on micro-XFM signal intensity data for Ca^{2+} in different tomato fruit tissues

Tomato	*n*	Overall fruit signal	Maximum signal	Seeds signal	Locular cavity signal	Placenta signal	Septa signal
Ca^{2+} supply (A)							
6 mM	6	35 b	62 b	18.3 b	4.5 a	10.33 a	18 b
18 mM	6	45.16 a	224.8 a	29 a	4.33 a	13.33 a	32.33 a
Na^{+} supply (B)							
0	6	41 a	138 b	19.167 b	4.83 a	11.5 a	22.3 b
16 mM	6	39.17 a	148.83 a	28.17 a	4 a	12.17 a	28 a
P values							
Ca^{2+} level (A)		***	***	*	NS	NS	***
Na^{+} level (B)		NS	*	*	NS	NS	*
A × B		NS	***	NS	NS	NS	**

Means followed by the same letter are not statistically significant (Tukey's Test, $p < 0.05$) and *, **, ***, and "NS" indicate significant differences at $p < 0.05$, $p < 0.01$, $p < 0.001$, and non-significant differences, respectively.

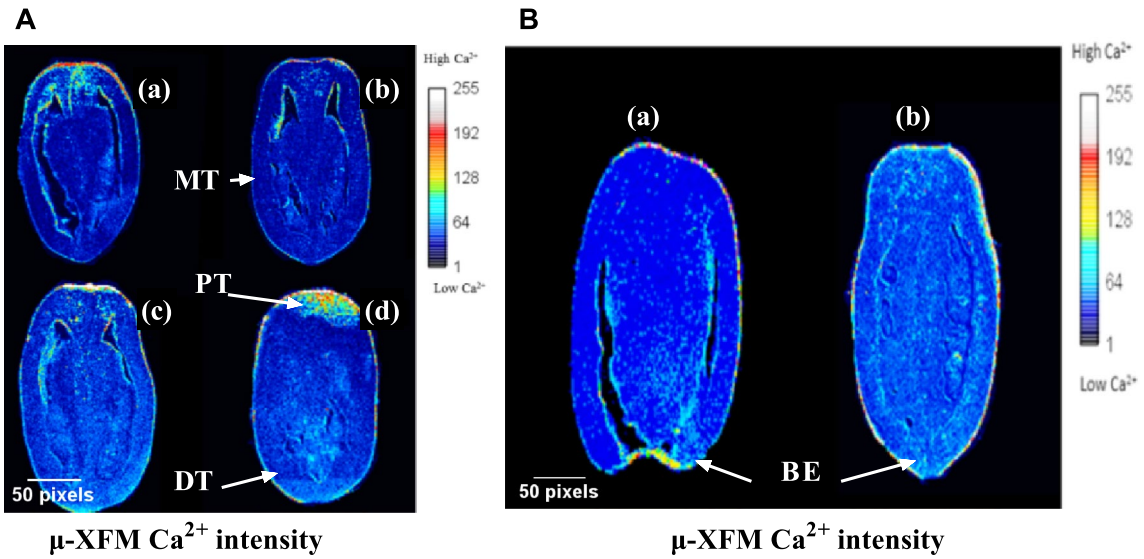

Fig. 9 Micro-XFM map showing spatial distribution patterns of calcium in 'Roma' tomato fruit. In the left panel, scans represent longitudinal orientation of 5 mm thick tissue from proximal to distal tissues. The plants received different calcium (Ca^{2+}; 6 and 18 mM) and sodium (Na^{+}; 0 and 16 mM) levels in irrigation solution. Letters a, b, c and d correspond to 6 mM Ca^{2+}/no Na^{+}, 6 Ca^{2+}/16 Na^{+} mM, 18 Ca^{2+}/no Na^{+} and 18 Ca^{2+}/16 mM Na^{+} treatments, respectively. The right-hand side picture shows Ca^{2+} distribution in fruit with blossom-end rot BER (**a**) versus a healthy fruit (**b**). PT: proximal tissues, MT: middle tissues, DT: distal tissues and BE: blossom end. The scans were conducted 76 days after salt imposition. Micro-XFM signal intensity representing concentration is shown as a colour scale. The original grayscale 8-bit maps were pseudo-coloured with a fire look-up table (LUT), colour range black (lowest signal) to white (brightest signal) as per the colour scale bars

the surface, Na^{+} accumulates in upper regions of growing media (Zhao et al. 2019).

Mechanical properties

It is important that the harvested tomato fruit has the ability to resist mechanical damage (Van Zeebroeck et al. 2007). Fruit have to withstand compression, impact, and abrasion throughout the postharvest supply chain (Li et al. 2017). Fruit strength in terms of load-bearing is related to Ca^{2+} cross-linking pectin towards rigidifying cell walls (Joyce et al. 2001; Park et al. 2005; Hocking et al. 2016). Braidwood et al. (2014) linked cell wall stiffness with composition and texture, particularly Ca^{2+}/pectin cross-linking. The hypothesis in the present experiment was that Ca^{2+} would displace Na^{+} at binding sites and improve fruit load bearing upon exposure to preharvest salinity and postharvest compression stresses. Na^{+} stress reportedly alters cell

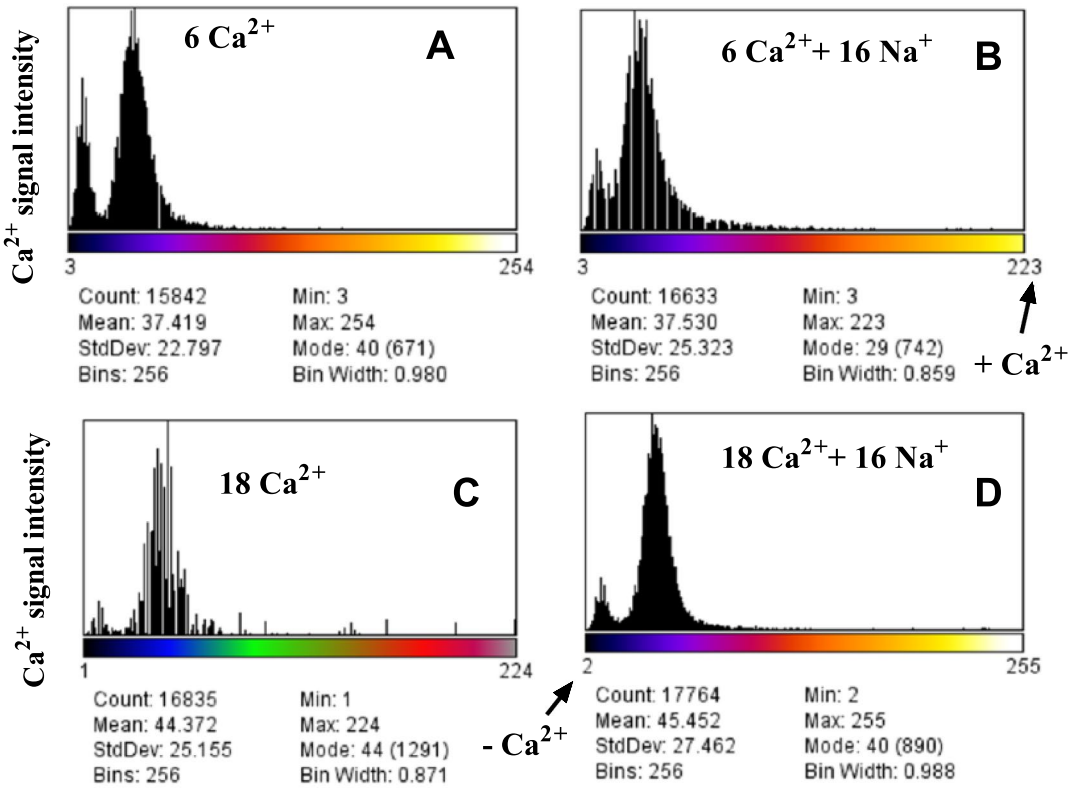

Fig. 10 Histogram plots of measured calcium concentrations and frequency of tomato fruit exposed to **a** 6 mM Ca^{2+}, **b** 6/16 Ca^{2+}/Na^{+}, **c** 18 Ca^{2+} and **d** 18/16 Ca^{2+}/Na^{+} in irrigation solution. The histogram graphs inform relative count, mean, peak, minimum Ca^{2+} signal intensity after 74 treatment days. Count is number of cells. Mean is the mean value. StdDev is the standard deviation. The Min and Max refer to the lowest and highest values of bins, respectively Bins is the number of the bins. Bin width is the width of each bin within the histogram. + Ca^{2+}; highest Ca^{2+} signal, − Ca^{2+}: lowest Ca^{2+} signal per treatment

wall properties in favour of cellular membrane deformation (Bose et al. 2011; Hamilton et al. 2015; Costan et al. 2020). Ca^{2+} within the apoplast is thus important for fruit strength (Höfte et al. 2012). From the results, Ca^{2+} supplementation in the irrigation solution enhanced all mechanical parameters. Namely, fruit were stiffer, which suggests greater Ca^{2+}—pectin cross-linking (Table 2). With 18 mM Ca^{2+} in the irrigation solution, tomato fruit flesh exhibited enhanced mechanical strength, including bending stretchability and penetration resistance. Nonetheless, mechanical properties of distal tissue remained relatively low even at maximum Ca^{2+} supplementation. This suggests non-uniform Ca^{2+} partitioning along the proximal to distal fruit axis (Table 2).

The results demonstrated that Na^{+} provokes susceptibility to tissue plastic damage in response to mechanical loading of tomato flesh (Table 2). The stretchability index or peak force before failure was lower for elevated Na^{+} treatments (Table 2) that concomitantly reduce Ca^{2+} in the distal tissue (Table 4). Hence cells prospectively begin to rupture at a lower bio-yield point compared to those from high Ca^{2+} treatments. Salinity thus appears to play an important role in flesh softness. Accumulating evidence suggests relationships between Na^{+} and cell wall deformation. For example, Tenhaken (2015) reported that Ca^{2+} crosslinking with pectic-gels is reduced when excess Na^{+} is present via irrigation. Similarly, Feng et al. (2016) reported that Na^{+} reduces wall rigidity and adversely affects the biosynthesis of new walls in terms of their pectin, xyloglucan, or cellulose composition, and may perturb cell wall and membrane association. Feng et al. (2018) reported that Na^{+} has a direct impact on mechanical properties of the root cell wall of *Arabidopsis thaliana* as affected by Na^{+} apoplastic toxicity.

When Na^{+} displaces pectin-bound Ca^{2+}, it characteristically disrupts pectin cross-linking (Byrt et al. 2018). Supplementation of Ca^{2+} in saline irrigation solution restored tomato fruit firmness, but not stiffness and peak force (Table 2). The latter characteristically reflects cell wall rigidity. Ottow et al. (2005) considered that cell walls absorb and stores excess Na^{+}, whereby it can displace Ca^{2+} and K^{+} at anionic binding sites. Together, the examined mechanical

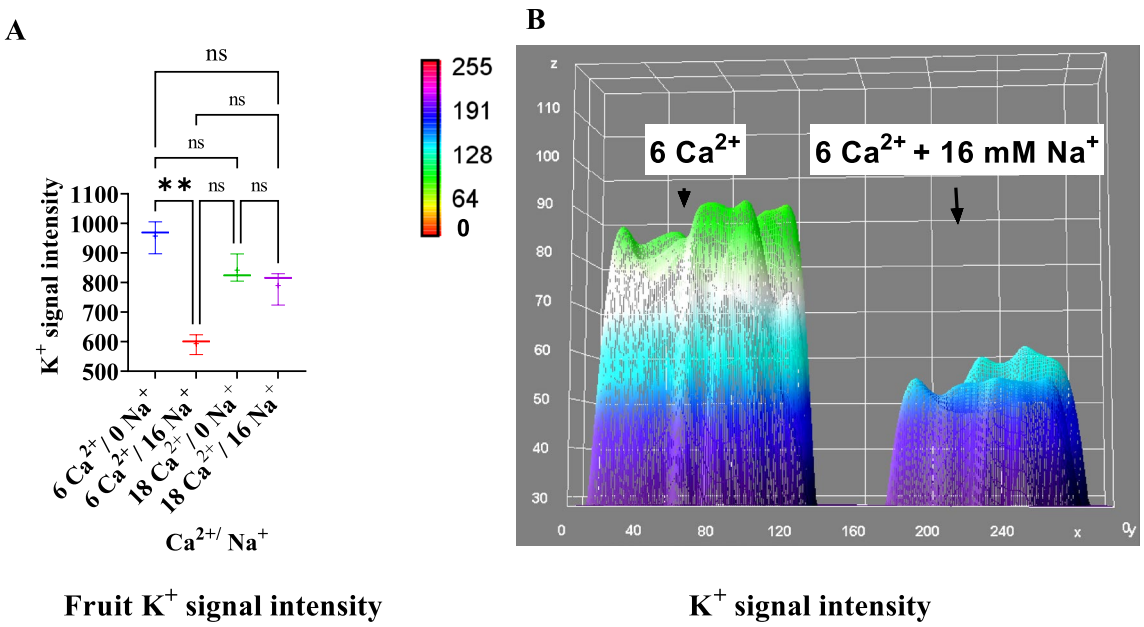

Fig. 11 X -ray fluorescence microscopy signal intensity of K^+ of 'Roma' tomato fruit as influenced by calcium (Ca^{2+}; 6 and 18 mM) and sodium (Na^+; 0 and 16 mM) in the irrigation solution (**A**), $n = 3$. Surface plots demonstrate the effect of added Na^+ (no added Na^+ *vs.* 16 mM Na^+) on the intensity and spatial distribution of potassium ($K.^+$) in tomato fruit (**B**). *, **, *** and "ns" indicate significant differences at $p < 0.05$, $p < 0.01$, $p < 0.001$, and non-significant differences, respectively. $N = 3$

properties data (Table 2) in the present study support the hypothesis that Ca^{2+} and Na^+ induce changes in the mechanical performance of tomato flesh.

Mineral partitioning

Spatiotemporal regulation of Ca^{2+} concentration is important for the mechanical properties and salt tolerance of fruit (Anino et al. 2006; Tuna et al. 2007; Hadi and Karimi 2012). As Ca^{2+} uptake is dependent not only on its supply from the roots, but also on its interactions with other cations in passage from soil to fruit (Reid and Smith 2000). In the present study, Ca^{2+}, K^+, and Mg^{2+} amounts markedly decreased in response to Na^+ supply (Table 3). Increased Ca^{2+}/Na^+ ratio may activate the uptake of other essential ions (Tuna et al. 2007). In the present study, Mg^{2+} concentrations increased with increased Ca^{2+} supply (Table 3). With 18 mM Ca^{2+} in the irrigation solution, Na^+ concentration in fruit flesh dropped in apparent association with enhanced K^+ over Na^+ (Table 3). At a finer level, Ca^{2+} ions also alter selectivity of cation channels to favour higher K^+/Na^+ selectivity (Shabala et al. 2006; Olias et al. 2009; Ragel et al. 2019). High K^+ is considered a main competitor of Na^+ entrance into the plant tissues (Olias et al. 2009). In the present study, an antagonistic effect between Ca^{2+} and Na^+ was evident (Table 3).

In the first experiment (Table 3), Ca^{2+} concentration distribution reflected uneven partitioning in the tomato fruit flesh. Ca^{2+} concentration fell along from the proximal to distal tissue gradient. An opposite increasing trend was discerned for K^+, P, and Mg^{2+} concentrations. For example, K^+ was 66-fold higher in concentration in the distal tissue than was Ca^{2+}. The declining gradient of Ca^{2+} concentrations from proximal pedicel end toward distal calyx end is consistent with Chen et al. (2019) for apples. Most nutrients are supplied through phloem vessels (Song et al. 2017; Van de Wal et al. 2017). However, phloem-immobile Ca^{2+} is supplied through the xylem system (Ho and White 2005; De Freitas et al. 2011; Gilliham et al. 2011). Montanaro et al. (2010) observed that 83% of Ca^{2+} content was secured during the first 4 weeks of apricot fruit growth, mainly via the xylem. In contrast, K^+ and Mg^{2+} uptake was sustained towards the end of fruit maturation stage via the phloem. A fast-growing low-transpiring fruit or organ may perhaps acquire more water via the phloem than via the xylem. Since Ca^{2+} is phloem immobile (Hocking et al. 2016), this leads to a lower Ca^{2+} uptake relative to sustained uptake of K^+ and Mg^{2+} through xylem vessels. Moreover, fruit lose xylem functionality during the rapid fruit expansion period,

particularly in their distal tissues (Song et al. 2018). This dysfunctionality reduces Ca^{2+} influx into and within fruit, leading to deficiency.

Calcium and potassium distribution within tomato leaflet and fruit tissues

Na^+ limited Ca^{2+} and K^+ concentrations in leaflet tissues (Fig. 6) as reflected in leaflet midrib and veins that had high K^+ reflected in pseudo green-scale image intensity in micro-XFM maps. By comparison, these intensities were relatively lower when Na^+ was included in the irrigation solution (Fig. 6). Supplemental Ca^{2+} alleviated the Na^+ toxicity such that concentrations of Ca^{2+} and K^+ were akin to those observed for control treatment. Munns and Tester (2008) suggest that Ca^{2+} can ameliorate Na^+ toxicity through enhancing K^+/Na^+ ratio uptake. In contrast, ICP-MS analyses revealed no such putative ameliorative effect of Ca^{2+} on K^+ under saline conditions (Table 4). The apparent contradiction is possibly because relatively coarse ICP-MS does not reflect finer spatial variation of K^+ across the leaflet. This result represents the utility of micro-XFM applied in plant nutrition studies towards better understanding.

Ca^{2+} and K^+ localization in leaflets varied. Ca^{2+} evidently accumulated towards the leaflet margins and tips. It moves passively through xylem in the transpiration stream to enter leaflet vein extensions (Kumar et al. 2015). Ca^{2+} then moves relatively slowly by mass flow through the apoplastic pathway to accumulate at leaf margins (Kumar et al. 2015). This distribution process explains higher concentrations of Ca^{2+} in the leaflet margins and apex as seen in the present study (Fig. 6). It also showed that Ca^{2+} retention in the midrib and veins is relatively low and that high K^+ corresponds with low Ca^{2+}, particularly in the midrib and veins (Fig. 6). This difference implies different distribution mechanisms between the two cations. Hence, contrasting localization of Ca^{2+} versus K^+ in the tomato terminal leaflet likely reflects their different modes of accumulation and redistribution; viz., via symplast *cf*. apoplast or phloem *cf*. xylem (Ragel et al. 2019). X-ray Microanalysis of citrus leaves (*Citrus jambhiri* Lush) elemental mapping demonstrated a distinct variation in Ca^{2+} and K^+ localization across different cell types (Storey and Leigh 2004). Ca^{2+} was primarily localized in the palisade and spongy mesophyll cells, exhibiting minimal presence in the epidermal and bundle sheath cells. Conversely, K^+ was mainly found in the epidermal and bundle sheath cells, with significantly lower levels detected in the palisade and spongy mesophyll cells. In contrast to K^+ uptake, Ca^{2+} is only absorbed by the xylem/apoplast pathway (Indeche et al. 2020). Furthermore, the different distributions of Ca^{2+} and K^+ within the palisade and spongy mesophyll cells could explain the observed differences in ions localization in the current experiment.

More generally in a botanical context, understanding Ca^{2+} distribution from soil application to plant organs is of importance to the fruit industry and consumers (Saure 2005; Kumar et al. 2015). Fruit are architecturally isolated organs (Hocking et al. 2016; Song et al. 2017, 2018). The pedicel or peduncle provides water and nutrients through the xylem and phloem. In fruit, Ca^{2+} distribution is modulated by the xylem system (Cieslak et al. 2016). In the present work, ICP-MS showed a decrease of Ca^{2+} concentrations from proximal to distal tissues associated with a drop in fruit stiffness and firmness (Table 2). Ca^{2+} in fruit mapping from proximal to distal and abaxial to adaxial (internal) was conducted in relation to salinity.

Micro-XFM revealed a decrease of Ca^{2+} from proximal to distal tissues as well as a decrease from exocarp through mesocarp to endocarp tissues. The exocarp is typically comprised of several layers of small collenchyma cells with dense cell wall network (Leroux 2012). By contrast, the mesocarp typically contains thin-walled cells of highly vacuolated parenchyma cells separated by intercellular spaces. That cell walls contain the largest (60–75%) pool of cell Ca^{2+} in plant tissues (Hyodo et al. 2013) may explain the higher Ca^{2+} signal intensity in exocarp tissues found (Table 6). Moreover, Moriwaki et al. (2014) observed that vasculature density and length is relatively higher towards the skin.

The different fruit parts differentially reflected Ca^{2+} and Na^+ irrigation treatments. Seed showed higher intensities of Ca^{2+} signals, while locular and placental tissues showed no increase in Ca^{2+} signal intensity in response to Ca^{2+} irrigation solution (Table 7). Higher signal intensities were observed in the septa with Ca^{2+}-enhanced solution (18 mM) compared to 6 mM Ca^{2+} solution. These observations are consistent with an ion-microprobe mass spectrometry study by Hyodo et al. (2013). Micro-XFM analysis was in concert with ICP-MS in reflecting a depressive effect of Na^+ on K^+ uptake in tomato flesh. Munns and Tester (2008) reported that elevated Na^+ restricts K^+ uptake. Unlike micro-XFM, ICP-MS analyses did not detect the increased tissue K^+ in tomato flesh as associated with Ca^{2+}-enhanced irrigation solution under salinity (Table 3). The limitations of ICP-MS analyses may stem from its inability to provide the same level of spatial resolution or detection limits that can be attained with XFM.

Calcium levels in distal fruit tissues were not elevated by the Ca^{2+}-enhanced irrigation solution in the current investigation. (Table 3; Fig. 9). Movement of water and nutrients into fruit depends on vascular distribution in the fruit (Cieslak et al. 2016). A strong xylem network provides water movement into fruit. Low Ca^{2+} in distal tissues (Table 4) is likely associated with progressive dysfunctionality of xylem connecting proximal peduncle to distal fruit tissues. Chen et al. (2019) studied the xylem functionality in Ca^{2+}-deficiency disorders of the calyx end of apples using methyl blue dye-infusion. With apple fruit ripening, no stained xylem was observed in distal tissues. In contrast, most xylem bundles near the proximal tissues were functioning. Similar findings were reported by Song et al. (2018) in different crops like loquat, apple, and pear. Moreover, Belda et al. (1996) found that Na^{+} disrupts tomato's fruit xylem and reduces the total xylem area in vascular bundles in distal tissue. Salinity reduced the average number of bundles by 33%. In this present study, that applied Ca^{2+} solution did not enhance Ca^{2+} levels in distal tissue were likely because of xylem functionality loss, particularly towards fruit ripening.

Calcium in healthy and blossom-end rot (BER) affected fruit

Distribution of Ca^{2+} along the abaxial–adaxial and proximal–distal axis was compared for healthy and BER-infected fruit. Despite increased Ca^{2+} in tomato flesh following Ca^{2+} supply treatments, all plants suffered Ca^{2+}-deficiency in developing BER-affected fruit (Table 1). Distal tissues had the lowest Ca^{2+} concentration, even when grown Ca^{2+}-enhanced irrigation solution. Daily VPD was 1.6 kPa in these experiments. A high VPD conditions favour rapid Ca^{2+} transport to highly transpiring leaves (Indeche et al. 2020) along with an increase in Ca^{2+} demand by growing fruit tissue (Tonetto de Freitas et al. 2014). The competition for Ca^{2+} between leaves and fruit triggers a lag or drop in Ca^{2+} transport to rapidly growing distal fruit tissue (Taylor and Locascio 2004; De Freitas et al. 2011; Tonetto de Freitas et al. 2014; Indeche et al. 2020; Matsumoto et al. 2021). Other cations, such as NH^{+}_{4}, Na^{+}, K^{+}, Mg^{2+}, and Mn^{2+} in solution interact with Ca^{2+} at binding sites, including on cell membranes (Reid and Smith 2000). Ionic competition, thereby, affects Ca^{2+} availability, uptake, translocation, and allocation to aboveground tissues (Reid and Smith 2000). Research suggests that nutrient concentration ratios, such as N^{+}/Ca^{2+}, K^{+}/Ca^{2+}, Mg^{2+}/Ca^{2+}, are useful indices of fruit Ca^{2+} nutrition status (Cramer 2002). ICP-MS, Ca^{2+} was 27-fold higher in leaves than fruit in the present study (Fig. 4). Of the total amount of Ca^{2+} allocated to fruit, only 19% was partitioned to distal tissues (Table 3). This reduction in Ca^{2+} concentration in distal tissues would continue to fall as fruit expand, ultimately leading to BER development.

Lastly, micro-XFM scans showed patches of Ca^{2+} in proximal tissue and along the exocarp, but relatively little such in distal tissues (Fig. 9). Micro-XFM analysis also showed fruit with visual BER symptoms had a fourfold increase in Ca^{2+} than in surrounding healthy tissue (Fig. 9). Val et al. (2008) using glyoxal bis (2-hydroxyanil; GBHA) to compare a healthy to bitter pit affected apple fruit found that the level of Ca^{2+} in bitter pit affected apples was threefold higher than in the adjacent sound tissue. In the present study, collapsed BER cells were likely remains of cells with walls rich in relatively immobile Ca^{2+}. Suzuki et al. (2003) showed that Ca^{2+} fed to tomato fruit increased in disintegrating BER tissue on the plasma membranes as the distance from the collapsed cells increased.

Conclusion

This study presents ICP-MS and micro-XFM imaging data that reflect Ca^{2+} distribution in leaflet and fruit tissues of tomato plants grown under varying salinity and Ca^{2+} supply conditions. Non-destructive WUE assessed under constant water table culture conditions fell over time regardless of salinity and Ca^{2+} levels. At low, but not high, salinity levels, additional Ca^{2+} mitigated softer fruit flesh otherwise induced by Na^{+}. Proximal fruit flesh tissues were firmer, stiffer, and showed higher resilience to mechanical deformation than distal tissues. Overall, higher than basal Ca^{2+} supply evidently ameliorated adverse Na^{+} effects reflected in increased Ca^{2+} and K^{+} concentrations in leaf and fruit tissues. Spatial mapping of Ca^{2+} by micro-XFM revealed K^{+} rich areas in leaflet midrib and veins that appear to correspond inversely with low Ca^{2+} concentrations. This inverse relationship implies competition between these two cations. Relatively limited mobility of Ca^{2+} in fruit was apparent under enhanced Ca^{2+} supply in terms of low levels in distal tissues. Also, Ca^{2+} was higher in exocarp compared with mesocarp tissues.

Appendix

See Figs. 12 and 13.

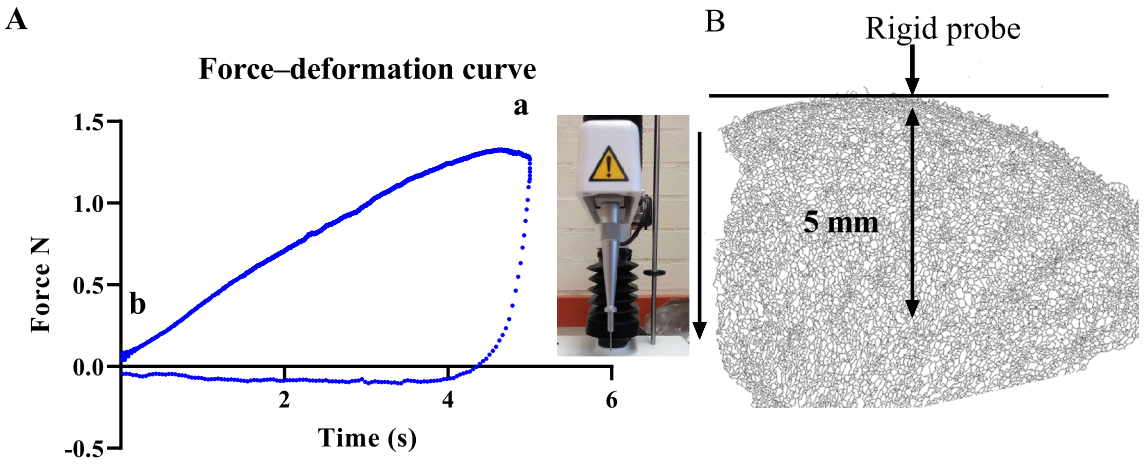

Fig. 12 Compression test with a rigid probe of tomato mesocarp without exocarp showing a typical force–deformation curve (a–b) of 5 mm and tissue failure point b (**A**). Fruit cross-section of apricot fruit showing the direction of the applied force to a depth of 5 mm (**B**), arrowhead indicates the applied force direction and double ended arrows indicate the probe penetration depth

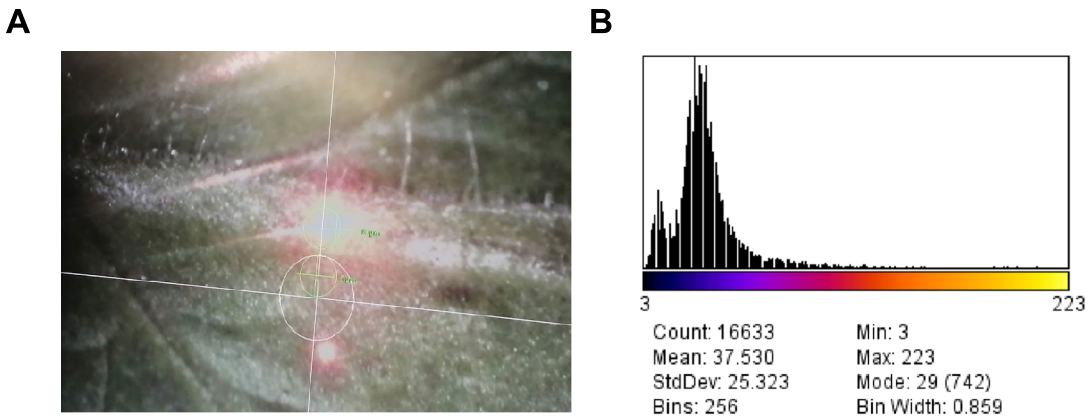

Fig. 13 **A** Showing the scanning of a 'Roma" tomato leaflet using the Iridium Ultra View Linescan Data (XFM) analysis package. **B** Histogram showing calcium signal peak, minimum, mean, and number of counts in a tomato leaflet grown in irrigation solution of a constant water table

Acknowledgements We thank Miss Katherine Raymont from School of Agriculture and Food Sustainability, Gatton, for help in processing the soil and plant samples and obtaining the nutrients concentrations. We also thank Lauchlan Casey from Centre for Microscopy and Microanalysis, The University of Queensland, for assistance with XFM analysis. The XFM analysis was undertaken at the Centre for Microscopy and Microanalysis (CMM) at the University of Queensland, Australia. We also thank Richard Webb for his general guidance in preparation of the plant samples for XFM analysis. Additionally, we gratefully acknowledge statistical advice and guidance kindly given by Dr. Vincent Mellor and Allan Lisle.

Author Contribution Abdullah Al Hosni: conceptualization, methodology, data curation, analysis, and writing original draft, software. Daryl Joyce: project administration, conceptualization, visualization, supervision, writing review and editing. Mal Hunter: data curation, methodology, supervision, conceptualization, experimental design, writing review and editing. Melinda Perkins: writing—review and editing, supervision. Rashid Al Yahyai: funding acquisition, writing review and editing, and supervision.

Funding Open Access funding enabled and organized by CAUL and its Member Institutions.

Data availability No datasets were generated or analysed during the current study.

Declarations

Competing interest The authors declare that they have no known competing financial interests or personal relationships that could have appeared to influence the work reported in this paper.

Open Access This article is licensed under a Creative Commons Attribution 4.0 International License, which permits use, sharing,

adaptation, distribution and reproduction in any medium or format, as long as you give appropriate credit to the original author(s) and the source, provide a link to the Creative Commons licence, and indicate if changes were made. The images or other third party material in this article are included in the article's Creative Commons licence, unless indicated otherwise in a credit line to the material. If material is not included in the article's Creative Commons licence and your intended use is not permitted by statutory regulation or exceeds the permitted use, you will need to obtain permission directly from the copyright holder. To view a copy of this licence, visit http://creativecommons.org/licenses/by/4.0/.

References

Alamar MC, Vanstreels E, Oey M, Moltó E, Nicolaï B (2008) Micromechanical behaviour of apple tissue in tensile and compression tests: Storage conditions and cultivar effect. J Food Eng 86(3):324–333. https://doi.org/10.1016/j.jfoodeng.2007.10.012

An X, Li Z, Zude-Sasse M, Tchuenbou-Magaia F, Yang Y (2020) Characterization of textural failure mechanics of strawberry fruit. J Food Eng 282:110016. https://doi.org/10.1016/j.jfoodeng.2020.110016

Anino SV, Salvatori DM, Alzamora SM (2006) Changes in calcium level and mechanical properties of apple tissue due to impregnation with calcium salts. Food Res Int 39(2):154–164. https://doi.org/10.1016/j.foodres.2005.07.003

Atkinson NJ, Dew TP, Orfila C, Urwin PE (2011) Influence of combined biotic and abiotic stress on nutritional quality parameters in tomato (*Solanum lycopersicum*). J Agric Food Chem 59(17):9673–9682. https://doi.org/10.1021/jf202081t

Belda RM, Fenlon J, Ho L (1996) Salinity effects on the xylem vessels in tomato fruit among cultivars with different susceptibilities to blossom-end rot. J Horticult Sci 71(2):173–179. https://doi.org/10.1080/14620316.1996.11515394

Besada C, Gil R, Bonet L, Quiñones A, Intrigliolo D, Salvador A (2016) Chloride stress triggers maturation and negatively affects the postharvest quality of persimmon fruit. Involvement of calyx ethylene production. Plant Physiol Biochem 100:105–112. https://doi.org/10.1016/j.plaphy.2016.01.006

Bose J, Pottosin I, Shabala S, Palmgren M, Shabala S (2011) Calcium efflux systems in stress signaling and adaptation in plants. Front Plant Sci 2(85). https://doi.org/10.3389/fpls.2011.00085

Braidwood L, Breuer C, Sugimoto K (2014) My body is a cage: mechanisms and modulation of plant cell growth. New Phytologist 201(2):388–402. https://doi.org/10.1111/nph.12473

Bui H-T, Makhlouf J, Ratti C (2010) Postharvest ripening characterization of greenhouse tomatoes. Int J Food Prop 13(4):830–846. https://doi.org/10.1080/10942910902895234

Byrt CS, Munns R, Burton RA, Gilliham M, Wege S (2018) Root cell wall solutions for crop plants in saline soils. Plant Sci 269:47–55. https://doi.org/10.1016/j.plantsci.2017.12.012

Camps C (2018) Singular approach to penetrometry by preprocessing of digitized force–displacement curves and chemometry: a case study of 12 tomato varieties. J Texture Stud 49(4):378–386. https://doi.org/10.1111/jtxs.12316

Cerri M, Reale L (2020) Anatomical traits of the principal fruits: an overview. Sci Hortic 270:109390. https://doi.org/10.1016/j.scienta.2020.109390

Chen S-J, Yeh D-M, Lin H-L, Li K-T (2019) Discontinuity of xylem function during maturation associated with quality development and calcium allocation in wax apple (*Syzygium samarangense* Merr. & Perry) fruit. FRUITS 74(3):117–123: https://doi.org/10.17660/th2019/74.3.3

Choi K, Lee G, Han Y, Bunn J (1995) Tomato maturity evaluation using color image analysis. Trans ASAE 38(1):171–176. https://doi.org/10.13031/2013.27827

Cieslak M, Cheddadi I, Boudon F, Baldazzi V, Génard M, Godin C, Bertin N (2016) Integrating physiology and architecture in models of fruit expansion. Front Plant Sci 7:1739. https://doi.org/10.3389/fpls.2016.01739

Costa A, Navazio L, Szabo I (2018) The contribution of organelles to plant intracellular calcium signalling. J Exp Bot 69(17):4175–4193. https://doi.org/10.1093/jxb/ery185

Costan A, Stamatakis A, Chrysargyris A, Petropoulos SA, Tzortzakis N (2020) Interactive effects of salinity and silicon application on *Solanum lycopersicum* growth, physiology and shelf-life of fruit produced hydroponically. J Sci Food Agric 100(2):732–743. https://doi.org/10.1002/jsfa.10076

Cramer GR (2002) Sodium-calcium interactions under salinity stress. In: Salinity: environment-plants-molecules. Springer, pp 205–227

Cybulska J, Zdunek A, Konstankiewicz K (2011) Calcium effect on mechanical properties of model cell walls and apple tissue. J Food Eng 102(3):217–223. https://doi.org/10.1016/j.jfoodeng.2010.08.019

Day KJ, John EA, Hutchings MJ (2003) The effects of spatially heterogeneous nutrient supply on yield, intensity of competition and root placement patterns in Briza media and *Festuca ovina*. Funct Ecol 17(4):454–463. https://doi.org/10.1046/j.1365-2435.2003.00758.x

Diels E, Wang Z, Nicolai B, Ramon H, Smeets B (2019) Discrete element modelling of tomato tissue deformation and failure at the cellular scale. Soft Matter 15(16):3362–3378. https://doi.org/10.1039/C9SM00149B

de Freitas ST, Jiang C-Z, Mitcham EJ (2012) Mechanisms involved in calcium deficiency development in tomato fruit in response to gibberellins. J Plant Growth Regul 31(2):221–234. https://doi.org/10.1007/s00344-011-9233-9

de Freitas ST, Padda M, Wu Q, Park S, Mitcham EJ (2011) Dynamic alternations in cellular and molecular components during blossom-end rot development in tomatoes expressing sCAX1, a constitutively active Ca^{2+}/H^{+} antiporter from Arabidopsis. Plant Physiol 156(2):844–855. https://doi.org/10.1104/pp.111.175208

De Kreij C, Voogt W, Van den Bos A, Baas R (1997) Voedingsoplossingen voor de teelt van tomaat in gesloten teeltsystemen. Brochure VG Tomaat, The Netherlands

Feng W, Kita D, Peaucelle A, Cartwright HN, Doan V, Duan Q, Liu MC, Maman J, Steinhorst L, Schmitz-Thom I, Yvon R, Kudla J, Wu HM, Cheung AY, Dinneny JR (2018) The FERONIA receptor kinase maintains cell-wall integrity during salt stress through Ca^{2+} signalling. Curr Biol 28(5):666–75.e5. https://doi.org/10.1016/j.cub.2018.01.023

Feng W, Lindner H, Robbins NE, Dinneny JR (2016) Growing out of stress: the role of cell- and organ-scale growth control in plant water-stress responses. Plant Cell 28(8):1769. https://doi.org/10.1105/tpc.16.00182

Flowers TJ, Munns R, Colmer TD (2015) Sodium chloride toxicity and the cellular basis of salt tolerance in halophytes. Ann Botany 115(3):419–4131. https://doi.org/10.1093/aob/mcu217

García J, Ruiz-Altisent M, Barreiro P (1995) Factors influencing mechanical properties and bruise susceptibility of apples and pears. J Agric Eng Res 61(1):11–17. https://doi.org/10.1006/jaer.1995.1025

Gilliham M, Dayod M, Hocking BJ, Xu B, Conn SJ, Kaiser BN, Leigh RA, Tyerman SD (2011) Calcium delivery and storage in plant leaves: exploring the link with water flow. J Exp Bot 62(7):2233–2250. https://doi.org/10.1093/jxb/err111

Giongo L, Ajelli M, Poncetta P, Ramos-García M, Sambo P, Farneti B (2019) Raspberry texture mechanical profiling during fruit ripening and storage. Postharvest Biol Technol 149:177–186. https://doi.org/10.1016/j.postharvbio.2018.11.021

Hadi MR, Karimi N (2012) The role of calcium in plants salt tolerance. J Plant Nutr 35(13):2037–2054. https://doi.org/10.1080/01904167.2012.717158

Hamilton ES, Schlegel AM, Haswell ES (2015) United in diversity: mechanosensitive ion channels in plants. Ann Rev Plant Biol 66:113–137. https://doi.org/10.1146/annurev-arplant-043014-114700

Ho LC, White PJ (2005) A cellular hypothesis for the induction of blossom-end rot in tomato fruit. Ann Botany 95(4):571–581. https://doi.org/10.1093/aob/mci065

Hocking B, Tyerman SD, Burton RA, Gilliham M (2016) Fruit calcium: transport and physiology. Front Plant Sci 7(569). https://doi.org/10.3389/fpls.2016.00569

Höfte H, Peaucelle A, Braybrook S (2012) Cell wall mechanics and growth control in plants: the role of pectins revisited. Front Plant Sci 3:121. https://doi.org/10.3389/fpls.2012.00121

Hrmova M, Gilliham M (2018) Plants fighting back: to transport or not to transport, this is a structural question. Curr Opin Plant Biol 46:68–76. https://doi.org/10.1016/j.pbi.2018.07.006

Hunter M, Leong G, Mitchell J, Dieters M, Fujinuma R (2018) Constant water table sub-irrigation of pots allows derivation of root weights (without physical recovery) and repeated measures of in situ growth and water use efficiencies. Plant Soil 425(1–2):1–19. https://doi.org/10.1007/s11104-017-3536-y

Hunter M, Scattini W (2014) The ANOVApot® and Twinpot reduce root escape and save water. In: XXIX International Horticultural Congress on Horticulture: Sustaining Lives, Livelihoods and Landscapes (IHC2014), 1112, pp 23–30. https://doi.org/10.17660/ActaHortic.2016.1112.4

Hyodo H, Terao A, Furukawa J, Sakamoto N, Yurimoto H, Satoh S, Iwai H (2013) Tissue specific localization of pectin–Ca^{2+} cross-linkages and pectin methyl-esterification during fruit ripening in tomato (*Solanum lycopersicum*). PLoS One 8(11). https://doi.org/10.1371/journal.pone.0078949

Indeche AK, Yoshida Y, Goto T, Yasuba K-I, Tanaka Y (2020) Effect of defoliation on blossom-end rot incidence and calcium transport into fruit of tomato cultivars under moderate water stress. Horticulture J 89(1):22–29. https://doi.org/10.2503/hortj.UTD-079

Islam MZ, Mele MA, Choi K-Y, Kang H-M (2018) Nutrient and salinity concentrations effects on quality and storability of cherry tomato fruits grown by hydroponic system. Bragantia 77:385–393. https://doi.org/10.1590/1678-4499.2017185

Joyce D, Shorter A, Hockings P (2001) Mango fruit calcium levels and the effect of postharvest calcium infiltration at different maturities. Sci Hortic 91(1–2):81–99. https://doi.org/10.1016/S0304-4238(01)00247-3

Kumar A, Singh UM, Manohar M, Gaur VS (2015) Calcium transport from source to sink: understanding the mechanism (s) of acquisition, translocation, and accumulation for crop biofortification. Acta Physiologiae Plantarum 37(1):1722. https://doi.org/10.1007/s11738-014-1722-6

Leroux O (2012) Collenchyma: a versatile mechanical tissue with dynamic cell walls. Ann Botany 110(6):1083–1098. https://doi.org/10.1093/aob/mcs186

Li Z, Li P, Liu J (2010) Effect of tomato internal structure on its mechanical properties and degree of mechanical damage. Afr J Biotechnol 9(12). https://doi.org/10.5897/AJB2010.000-3020

Li Z, Li P, Yang H, Liu J, Xu Y (2012) Mechanical properties of tomato exocarp, mesocarp and locular gel tissues. J Food Eng 111(1):82–91. https://doi.org/10.1016/j.jfoodeng.2012.01.023

Li Z, Miao F, Andrews J (2017) Mechanical models of compression and impact on fresh fruits. Comprehens Rev Food Sci Food Safety 16(6):1296–312. https://doi.org/10.1111/1541-4337.12296

Li Z, Thomas C (2014) Quantitative evaluation of mechanical damage to fresh fruits. Trends Food Sci Technol 35(2):138–150. https://doi.org/10.1016/j.tifs.2013.12.001

Liu S, Yang H, Bian Z, Tao R, Chen X, Lu TJ (2019) Regulation on mechanical properties of spherically cellular fruits under osmotic stress. J Mech Phys Solids 127:182–190. https://doi.org/10.1016/j.jmps.2019.03.007

Lovelli S, Scopa A, Perniola M, Di Tommaso T, Sofo A (2012) Abscisic acid root and leaf concentration in relation to biomass partitioning in salinized tomato plants. J Plant Physiol 169(3):226–233. https://doi.org/10.1016/j.jplph.2011.09.009

Matsumoto C, Yada H, Hayakawa C, Hoshino K, Hirai H, Kato K, Ikeda H (2021) Physiological characterization of tomato introgression line IL5-4 that increases brix and blossom-end rot in ripening fruit. Horticulture J: UTD-264. https://doi.org/10.2503/hortj.UTD-264

McNickle GG, Deyholos MK, Cahill JF Jr (2016) Nutrient foraging behaviour of four co-occurring perennial grassland plant species alone does not predict behaviour with neighbours. Funct Ecol 30(3):420–430. https://doi.org/10.1111/1365-2435.12508

Moles TM, de Brito FR, Mariotti L, Pompeiano A, Lupini A, Incrocci L, Carmassi G, Scartazza A, Pistelli L, Guglielminetti L (2019) Salinity in autumn-winter season and fruit quality of tomato landraces. Front Plant Sci 10:1078. https://doi.org/10.3389/fpls.2019.01078

Molina-Montenegro MA, Acuña-Rodríguez IS, Torres-Díaz C, Gundel PE, Dreyer I (2020) Antarctic root endophytes improve physiological performance and yield in crops under salt stress by enhanced energy production and Na^+ sequestration. Sci Rep 10(1):1–10. https://doi.org/10.1038/s41598-020-62544-4

Montanaro G, Dichio B, Xiloyannis C (2010) Significance of fruit transpiration on calcium nutrition in developing apricot fruit. J Plant Nutr Soil Sci 173(4):618–622. https://doi.org/10.1002/jpln.200900376

Moriwaki S, Terada Y, Kose K, Haishi T, Sekozawa Y (2014) Visualization and quantification of vascular structure of fruit using magnetic resonance microimaging. Appl Magn Reson 45(6):517–525. https://doi.org/10.1007/s00723-014-0537-3

Munns R, Tester M (2008) Mechanisms of salinity tolerance. Annu Rev Plant Biol 59:651–681. https://doi.org/10.1146/annurev.arplant.59.032607.092911

Navarro JM, Martıínez V, Carvajal M (2000) Ammonium, bicarbonate and calcium effects on tomato plants grown under saline conditions. Plant Sci 157(1):89–96. https://doi.org/10.1016/S0168-9452(00)00272-7

Olias R, Eljakaoui Z, Li J, De Morales PA, Marin-Manzano MC, Pardo JM, Belver A (2009) The plasma membrane Na^+/H^+ antiporter SOS1 is essential for salt tolerance in tomato and affects the partitioning of Na+ between plant organs. Plant Cell Environ 32(7):904–916. https://doi.org/10.1111/j.1365-3040.2009.01971.x

Ottow EA, Brinker M, Teichmann T, Fritz E, Kaiser W, Brosché M, Kangasjärvi J, Jiang X, Polle A (2005) Populus euphratica displays apoplastic sodium accumulation, osmotic adjustment by decreases in calcium and soluble carbohydrates, and develops leaf succulence under salt stress. Plant Physiol 139(4):1762–1772. https://doi.org/10.1104/pp.105.069971

Park S, Cheng NH, Pittman JK, Yoo KS, Park J, Smith RH, Hirschi KD (2005) Increased calcium levels and prolonged shelf life in tomatoes expressing Arabidopsis H^+/Ca^{2+} transporters. Plant Physiol 139(3):1194–1206. https://doi.org/10.1104/pp.105.066266

Peaucelle A, Braybrook S, Höfte H (2012) Cell wall mechanics and growth control in plants: the role of pectins revisited. Front Plant Sci 3:121. https://doi.org/10.3389/fpls.2012.00121

Peaucelle A, Wightman R, Höfte H (2015) The control of growth symmetry breaking in the Arabidopsis hypocotyl. Curr Biol 25(13):1746–1752. https://doi.org/10.1016/j.cub.2015.05.022

Perelman A, Jorda H, Vanderborght J, Lazarovitch N (2020) Tracing root-felt sodium concentrations under different transpiration rates

and salinity levels. Plant Soil 447(1):55–71. https://doi.org/10.1007/s11104-019-03959-5
Petersen KK, Willumsen J, Kaack K (1998) Composition and taste of tomatoes as affected by increased salinity and different salinity sources. J Hortic Sci Biotechnol 73(2):205–215. https://doi.org/10.1080/14620316.1998.11510966
Prieto I, Armas C, Pugnaire FI (2012) Hydraulic lift promotes selective root foraging in nutrient-rich soil patches. Functional Plant Biol 39(9):804–812. https://doi.org/10.1071/FP12070
Ragel P, Raddatz N, Leidi EO, Quintero FJ, Pardo JM (2019) Regulation of K^+ nutrition in plants. Front Plant Sci 10. https://doi.org/10.3389/fpls.2019.00281
Reid RJ, Smith FA (2000) The limits of sodium/calcium interactions in plant growth. Funct Plant Biol 27(7):709–715. https://doi.org/10.1071/PP00030
Reina-Sánchez A, Romero-Aranda R, Cuartero J (2005) Plant water uptake and water use efficiency of greenhouse tomato cultivars irrigated with saline water. Agric Water Manage 78(1–2):54–66. https://doi.org/10.1016/j.agwat.2005.04.021
Riboldi LB, Araújo SHdC, de Freitas ST, Camargo e Castro PRd (2018) Incidence of blossom-end rot in elongated tomato fruit. Botany 96(10):663–673. https://doi.org/10.1139/cjb-2018-0021
Ruiz MS, Yasuor H, Ben-Gal A, Yermiyahu U, Saranga Y, Elbaum R (2015) Salinity induced fruit hypodermis thickening alters the texture of tomato (*Solanum lycopersicum* Mill) fruits. Sci Hortic 192:244–249. https://doi.org/10.1016/j.scienta.2015.06.002
Saure MC (2005) Calcium translocation to fleshy fruit: its mechanism and endogenous control. Sci Hortic 105(1):65–89. https://doi.org/10.1016/j.scienta.2004.10.003
Schoonover JE, Crim JF (2015) An introduction to soil concepts and the role of soils in watershed management. J Contemp Water Res Educ 154(1):21–47. https://doi.org/10.1111/j.1936-704X.2015.03186.x
Shabala S, Demidchik V, Shabala L, Cuin TA, Smith SJ, Miller AJ, Davies JM, Newman IA (2006) Extracellular Ca^{2+} ameliorates NaCl-induced K+ loss from Arabidopsis root and leaf cells by controlling plasma membrane K^+-permeable channels. Plant Physiol 141(4):1653–1665. https://doi.org/10.1104/pp.106.082388
Song W, Yi J, Kurniadinata OF, Wang H, Huang X (2018) Linking fruit Ca uptake capacity to fruit growth and pedicel anatomy, a cross-species study. Front Plant Sci 9:575. https://doi.org/10.3389/fpls.2018.00575
Song WP, Chen W, Yi JW, Wang HC, Huang XM (2017) Ca distribution pattern in litchi fruit and pedicel and impact of Ca Channel Inhibitor, La(3). Front Plant Sci 8:2228. https://doi.org/10.3389/fpls.2017.02228
Stael S, Wurzinger B, Mair A, Mehlmer N, Vothknecht UC, Teige M (2012) Plant organellar calcium signalling: an emerging field. J Exp Bot 63(4):1525–1542. https://doi.org/10.1093/jxb/err394
Stopa R, Szyjewicz D, Komarnicki P, Kuta Ł (2018) Determining the resistance to mechanical damage of apples under impact loads. Postharvest Biol Technol 146:79–89. https://doi.org/10.1016/j.postharvbio.2018.08.016
Storey R, Leigh RA (2004) Processes modulating calcium distribution in citrus leaves. An investigation using X-ray microanalysis with strontium as a tracer. Plant Physiol 136:3838–3848. https://doi.org/10.1104/pp.104.045674
Suzuki K, Shono M, Egawa Y (2003) Localization of calcium in the pericarp cells of tomato fruits during the development of blossom-end rot. Protoplasma 222(3–4):149–156. https://doi.org/10.1007/s00709-003-0018-2
Tang H, Zhang X, Gong B, Yan Y, Shi Q (2020) Proteomics and metabolomics analysis of tomato fruit at different maturity stages and under salt treatment. Food Chem 311:126009. https://doi.org/10.1016/j.foodchem.2019.126009
Tattini M, Traversi ML (2009) On the mechanism of salt tolerance in olive (*Olea europaea* L.) under low-or high-Ca^{2+} supply. Environ Exp Bot 65(1):72–81. https://doi.org/10.1016/j.envexpbot.2008.01.005
Taylor MD, Locascio SJ (2004) Blossom-end rot: a calcium deficiency. J Plant Nutr 27(1):123–139. https://doi.org/10.1081/PLN-120027551
Tenhaken R (2015) Cell wall remodeling under abiotic stress. Front Plant Sci 5:771. https://doi.org/10.3389/fpls.2014.00771
Tonetto de Freitas S, McElrone AJ, Shackel KA, Mitcham EJ (2014) Calcium partitioning and allocation and blossom-end rot development in tomato plants in response to whole-plant and fruit-specific abscisic acid treatments. J Exp Bot 65(1):235–247. https://doi.org/10.1093/jxb/ert364
Tonina L, Giomi F, Sancassani M, Ajelli M, Mori N, Giongo L (2020) texture features explain the susceptibility of grapevine cultivars to *Drosophila suzukii* (Diptera: Drosophilidae) infestation in ripening and drying grapes. Sci Rep 10(1):1–13. https://doi.org/10.1038/s41598-020-66567-9
Tuna AL, Kaya C, Ashraf M, Altunlu H, Yokas I, Yagmur B (2007) The effects of calcium sulphate on growth, membrane stability and nutrient uptake of tomato plants grown under salt stress. Environ Exper Botany 59(2):173–178. https://doi.org/10.1016/j.envexpbot.2005.12.007
Val J, Gracia M, Monge E, Blanco A (2008) Visual detection of calcium by GBHA staining in bitter pit-affected apples. Food Sci Technol Int 14(4):315–319. https://doi.org/10.1177/1082013208097191
Van de Wal BA, Windt CW, Leroux O, Steppe K (2017) Heat girdling does not affect xylem integrity: an in vivo magnetic resonance imaging study in the tomato peduncle. New Phytol 215(2):558–568. https://doi.org/10.1111/nph.14610
Van der Ent A, Przybyłowicz WJ, de Jonge MD, Harris HH, Ryan CG, Tylko G, Paterson DJ, Barnabas AD, Kopittke PM, Mesjasz-Przybyłowicz J (2018) X-ray elemental mapping techniques for elucidating the ecophysiology of hyperaccumulator plants. New Phytol 218(2):432–452. https://doi.org/10.1111/nph.14810
Van Zeebroeck M, Darius P, De Ketelaere B, Ramon H, Tijskens E (2007) The effect of fruit properties on the bruise susceptibility of tomatoes. Postharvest Biol Technol 45(2):168–175. https://doi.org/10.1016/j.postharvbio.2006.12.022
Vang-Petersen O (1980) Calcium, potassium and magnesium nutrition and their interactions in 'Cox's Orange' apple trees. Sci Hortic 12(2):153–161. https://doi.org/10.1016/0304-4238(80)90122-3
Wan S, Kang Y, Wang D, Liu S-P, Feng L-P (2007) Effect of drip irrigation with saline water on tomato (*Lycopersicon esculentum* Mill) yield and water use in semi-humid area. Agric Water Manag 90(1–2):63–74. https://doi.org/10.1016/j.agwat.2007.02.011
Wang D, Yeats TH, Uluisik S, Rose JK, Seymour GB (2018) Fruit softening: revisiting the role of pectin. Trends Plant Sci 23(4):302–310. https://doi.org/10.1016/j.tplants.2018.01.006
Winisdorffer G, Musse M, Quellec S, Barbacci A, Gall SL, Mariette F, Lahaye M (2015) Analysis of the dynamic mechanical properties of apple tissue and relationships with the intracellular water status, gas distribution, histological properties and chemical composition. Postharvest Biol Technol 104:1–16. https://doi.org/10.1016/j.postharvbio.2015.02.010
Yang H, Shukla MK, Mao X, Kang S, Du T (2019) Interactive regimes of reduced irrigation and salt stress depressed tomato water use

efficiency at leaf and plant scales by affecting leaf physiology and stem sap flow. Front Plant Sci 10. https://doi.org/10.3389/fpls.2019.00160

Zhao X, Xia J, Chen W, Chen Y, Fang Y, Qu F (2019) Transport characteristics of salt ions in soil columns planted with *Tamarix chinensis* under different groundwater levels. PLoS ONE 14(4):e0215138. https://doi.org/10.1371/journal.pone.0215138

Zipori I, Dag A, Tugendhaft Y, Birger R (2014) Mechanical harvesting of table olives: harvest efficiency and fruit quality. HortScience 49(1):55–58. https://doi.org/10.21273/HORTSCI.49.1.55

Publisher's Note Springer Nature remains neutral with regard to jurisdictional claims in published maps and institutional affiliations.